Long-time behaviour of discretizations of the simple pendulum equation

2009 J. Phys. A: Math. Theor. 42 105204

(http://iopscience.iop.org/1751-8121/42/10/105204)

IOP PUBLISHING JOURNAL OF PHYSICS A: MATHEMATICAL AND THEORETICAL

J. Phys. A: Math. Theor. **42** (2009) 105204 (29pp) doi:10.1088/1751-8113/42/10/105204

Long-time behaviour of discretizations of the simple pendulum equation

Jan L Cieśliński[1] **and Bogusław Ratkiewicz**[21]

[11] Uniwersytet w Białymstoku, Wydział Fizyki, ul. Lipowa 41, 15-424 Białystok, Poland
[22] Doctoral Studies, Wydział Fizyki, Uniwersytet Adama Mickiewicza, Poznań, Poland

E-mail: janek@alpha.uwb.edu.pl and bograt@poczta.onet.pl

Received 6 December 2008, in final form 12 January 2009
Published 13 February 2009
Online at stacks.iop.org/JPhysA/42/105204

Abstract
We compare several discretizations of the simple pendulum equation in a series of numerical experiments. The stress is put on the long-time behaviour. The chosen numerical schemes are either symplectic maps or integrable (energy-preserving) maps, or both. Therefore, they preserve qualitative features of solutions (such as periodicity). We describe characteristic periodic time dependences of numerical estimates of the period and the amplitude, and explain them as systematic numerical by-effects produced by any method. Finally, we propose a new numerical scheme which is a modification of the discrete gradient method. This modified discrete gradient method preserves (almost exactly) the period of small oscillations for any time step.

PACS numbers: 45.10.−b, 02.60.Cb, 02.70.−c, 02.70.Bf
Mathematics Subject Classification: 65P10, 65L12, 34K28

1. Introduction

A new but increasingly important direction in numerical analysis is geometric numerical integration [11, 12, 14, 19]. Numerical methods within this approach are tailored for specific equations rather than for large general classes of equations. The aim is to preserve qualitative features, invariants and geometric properties of studied equations, e.g., integrals of motion, long-time behaviour and sometimes even trajectories (but it is difficult, sometimes even impossible, to preserve all properties by a single numerical scheme). 'Although the apparent desirability of this practice might be obvious at first glance, it nonetheless calls for a justification' [13].

In this paper, we perform a series of numerical experiments comparing the performance of several standard and geometric methods on the example of the simple pendulum equation.

[1] Permanent address: I LO, ul. Śródmieście 31, 16-300 Augustów, Poland.

The equation itself is very well known but its discrete counterparts show many interesting and unexpected features, for instance, the appearance of chaotic behaviour for large time steps [7, 29]. We focus our attention on the stability and time step dependence of the period and the amplitude for several discretizations of the simple pendulum (assuming that the time step is sufficiently small). We describe and explain small periodic oscillations of the period and of the amplitude around their average values.

We confine our studies either to symplectic maps or to energy-preserving maps. It is well known that symplectic integrators are very stable as far as the conservation of the energy is concerned. Since the beginning of 1990s they have been successfully used in the long-time integration of the solar system [27–29]; see also [4, 9]. The reason is that using any symplectic scheme of nth order the error of the Hamiltonian for an exponentially long time is of the order $O(\varepsilon^n)$, where ε is the constant step of the integration [3, 11, 18]. Therefore, in the studies of the long-time behaviour, symplectic algorithms have a great advantage at the very beginning. Fortunately, the class of symplectic integrators includes such well-known and relatively simple numerical schemes as the standard leap-frog method and the implicit midpoint rule. In this paper, we compare these classical methods with new geometric methods which preserve the energy integral.

We also propose a new discretization (a modification of the discrete gradient method) which is almost exact for small oscillations (even for large time steps) and keeps outstanding properties of the discrete gradient method (e.g., its precision in describing motions in the neighbourhood of the separatrix).

2. Symplectic discretizations of Newton equations

We consider scalar autonomous Newton equations:

$$\ddot{\varphi} = f(\varphi), \tag{1}$$

which can be written as the following first-order system:

$$\dot{\varphi} = p, \qquad \dot{p} = f(\varphi). \tag{2}$$

The equations are integrable for any function $f = f(\varphi)$ (in this case by integrability we mean the existence of the integral of motion; compare [26]). The energy conservation law reads

$$\frac{1}{2}\dot{\varphi}^2 + V(\varphi) = E, \qquad f(\varphi) = -\frac{\mathrm{d}V(\varphi)}{\mathrm{d}\varphi}, \tag{3}$$

where $E = \text{const}$. The Hamiltonian is given by

$$H(p, q) = \frac{p^2}{2} + V(q). \tag{4}$$

As an example to test quantitatively various numerical methods we will use the simple pendulum equation

$$\ddot{\varphi} = -k \sin\varphi. \tag{5}$$

In this case, the energy conservation law has the form

$$\tfrac{1}{2}p^2 - k\cos\varphi = E. \tag{6}$$

The constant k is not important. It can be eliminated by a change of the variable t. In the sequel (in any numerical computations) we assume $k = 1$.

By the discretization of (1) we mean an ε-family of difference equations (of the second order) which in the continuum limit $\varepsilon \to 0$ yields (1). The initial conditions should be discretized as well, i.e., we have to map $\varphi(0) \mapsto \varphi_0$, $\dot{\varphi}(0) \mapsto p_0$.

It is convenient to discretize (2) which automatically gives the discretization of p. Thus we have an ε-dependent map, $(\varphi_n, p_n) \mapsto (\varphi_{n+1}, p_{n+1})$. This map is called symplectic if for any n

$$\mathrm{d}\varphi_{n+1} \wedge \mathrm{d}p_{n+1} = \mathrm{d}\varphi_n \wedge \mathrm{d}p_n. \tag{7}$$

The following lemmas give a convenient characterization of symplectic maps, and we will apply them in the following sections.

Lemma 1. *The map* $(\varphi_n, p_n) \mapsto (\varphi_{n+1}, p_{n+1})$, *implicitly defined by*

$$\varphi_{n+1} - \varphi_n = P(p_n, p_{n+1}, \varepsilon), \quad p_{n+1} - p_n = R(\varphi_n, \varphi_{n+1}, \varepsilon), \tag{8}$$

where P and R are differentiable functions, is symplectic if and only if

$$\frac{\partial P}{\partial p_n}\frac{\partial R}{\partial \varphi_n} = \frac{\partial P}{\partial p_{n+1}}\frac{\partial R}{\partial \varphi_{n+1}} \neq 1. \tag{9}$$

The proof is straightforward. Differentiating (8) we get

$$\mathrm{d}\varphi_{n+1} - \mathrm{d}\varphi_n = P_{,1}\ \mathrm{d}p_n + P_{,2}\ \mathrm{d}p_{n+1},$$
$$\mathrm{d}p_{n+1} - \mathrm{d}p_n = R_{,1}\ \mathrm{d}\varphi_n + R_{,2}\ \mathrm{d}\varphi_{n+1},$$

(where the comma denotes the partial differentiation). Then

$$\mathrm{d}\varphi_{n+1} = \frac{1 + P_{,2}\ R_{,1}}{1 - P_{,2}\ R_{,2}}\,\mathrm{d}\varphi_n + \frac{P_{,1} + P_{,2}}{1 - P_{,2}\ R_{,2}}\,\mathrm{d}p_n,$$
$$\mathrm{d}p_{n+1} = \frac{R_{,1} + R_{,2}}{1 - P_{,2}\ R_{,2}}\,\mathrm{d}\varphi_n + \frac{1 + P_{,1}\ R_{,2}}{1 - P_{,2}\ R_{,2}}\,\mathrm{d}p_n,$$

provided that $P_{,2}\ R_{,2} \neq 1$ (this condition means that the map defined by P, R is non-degenerate). Therefore

$$\mathrm{d}\varphi_{n+1} \wedge \mathrm{d}p_{n+1} = \frac{1 - P_{,1}\ R_{,1}}{1 - P_{,2}\ R_{,2}}\,\mathrm{d}\varphi_n \wedge \mathrm{d}p_n.$$

Hence the map is symplectic if $P_{,1}\ R_{,1} = P_{,2}\ R_{,2} \neq 1$ which ends the proof.

Lemma 2. *The map* $(\varphi_n, p_n) \mapsto (\varphi_{n+1}, p_{n+1})$, *defined by*

$$\varphi_{n+1} - A(\varphi_n, \varepsilon) + \varphi_{n-1} = 0, \qquad p_n = \mu_0(\varepsilon)\varphi_{n+1} + B(\varphi_n, \varepsilon), \tag{10}$$

is symplectic for any differentiable functions A, B.

In order to prove lemma 2 we compute

$$\mathrm{d}p_{n+1} = \mu_0\,\mathrm{d}\varphi_{n+2} + TB'\,\mathrm{d}\varphi_{n+1} = \mu_0 TA'\,\mathrm{d}\varphi_{n+1} - \mu_0\,\mathrm{d}\varphi_n + TB'\,\mathrm{d}\varphi_{n+1},$$

where the prime denotes the differentiation, and T denotes the shift, i.e., $TA(\varphi_n) = A(\varphi_{n+1})$. Therefore

$$\mathrm{d}\varphi_{n+1} \wedge \mathrm{d}p_{n+1} = -\mu_0\,\mathrm{d}\varphi_{n+1} \wedge \mathrm{d}\varphi_n.$$

On the other hand, $\mathrm{d}\varphi_n \wedge \mathrm{d}p_n = \mu_0\,\mathrm{d}\varphi_n \wedge \mathrm{d}\varphi_{n+1}$, which ends the proof.

3. Non-integrable symplectic discretizations

In this section, we present some well-known discretizations which preserve the symplectic structure of the Newton equations (compare [11], pp 189–90) but have no integrals of motion.

3.1. Standard discretization

The standard discretization of the simple pendulum equation

$$\frac{\varphi_{n+1} - 2\varphi_n + \varphi_{n-1}}{\varepsilon^2} = -k \sin \varphi_n \tag{11}$$

is non-integrable [26]. This discretization can be obtained by the application of either the leap-frog (Störmer–Verlet) scheme or one of the symplectic Euler methods. It is interesting that we get the same discrete equation (11) but a different dependence of p_n on φ_n, φ_{n+1} (compare (16), (22)):

$$p_n = \frac{\varphi_{n+1} - \varphi_n}{\varepsilon} + ck\varepsilon \sin \varphi_n = \frac{\varphi_{n+1} - \varphi_{n-1}}{2\varepsilon} + \left(c - \frac{1}{2}\right) k\varepsilon \sin \varphi_n, \tag{12}$$

where $c = 0, \frac{1}{2}, 1$. By virtue of lemma 2 standard discretizations are symplectic (for any c).

3.2. The Störmer–Verlet (leap-frog) scheme

The numerical integration scheme

$$\begin{cases} p_{n+\frac{1}{2}} = p_n + \frac{1}{2}\varepsilon f(\varphi_n), \\ \varphi_{n+1} = \varphi_n + \varepsilon p_{n+\frac{1}{2}}, \\ p_{n+1} = p_{n+\frac{1}{2}} + \frac{1}{2}\varepsilon f(\varphi_{n+1}), \end{cases} \tag{13}$$

is known as the Störmer–Verlet (or leap-frog) method (compare, e.g., [11]). Eliminating $p_{n+\frac{1}{2}}$, we can easily formulate the Störmer–Verlet as a one-step method:

$$\begin{aligned} \varphi_{n+1} &= \varphi_n + \varepsilon p_n + \tfrac{1}{2}\varepsilon^2 f(\varphi_n), \\ p_{n+1} &= p_n + \tfrac{1}{2}\varepsilon \left(f(\varphi_n) + f\left(\varphi_n + \varepsilon p_n + \tfrac{1}{2}\varepsilon^2 f(\varphi_n)\right)\right). \end{aligned} \tag{14}$$

We can also formulate this method as

$$\frac{\varphi_{n+1} - 2\varphi_n + \varphi_{n-1}}{\varepsilon^2} = f(\varphi_n), \tag{15}$$

$$p_n = \frac{\varphi_{n+1} - \varphi_n}{\varepsilon} - \frac{\varepsilon}{2} f(\varphi_n). \tag{16}$$

In the simple pendulum case ($f(\varphi) = -k \sin \varphi$) we recognize in equations (15), (16) the standard discretization (11), (12) with $c = 1/2$.

3.3. Symplectic Euler methods

The system (2) belongs to the class of 'partitioned systems' which have the form

$$\dot{\varphi} = g(\varphi, p), \qquad \dot{p} = h(\varphi, p), \tag{17}$$

where g, h are given functions of two variables. We can discretize such systems in one of the following two ways:

$$\varphi_{n+1} = \varphi_n + \varepsilon g(\varphi_n, p_{n+1}), \qquad p_{n+1} = p_n + \varepsilon h(\varphi_n, p_{n+1}), \tag{18}$$

$$\varphi_{n+1} = \varphi_n + \varepsilon g(\varphi_{n+1}, p_n), \qquad p_{n+1} = p_n + \varepsilon h(\varphi_{n+1}, p_n). \tag{19}$$

Both these discretizations are called either symplectic Euler methods [11] or symplectic splitting methods [21]. In our case (see (2)) we have, respectively,

$$\varphi_{n+1} = \varphi_n + \varepsilon p_{n+1}, \qquad p_{n+1} = p_n + \varepsilon f(\varphi_n), \tag{20}$$

$$\varphi_{n+1} = \varphi_n + \varepsilon p_n, \qquad p_{n+1} = p_n + \varepsilon f(\varphi_{n+1}). \tag{21}$$

Finally, both (20) and (21) yield (15), but instead of (16) we have

$$p_n = \frac{\varphi_{n+1} - \varphi_n}{\varepsilon} - \varepsilon f(\varphi_n) \qquad \text{or} \qquad p_n = \frac{\varphi_{n+1} - \varphi_n}{\varepsilon}, \tag{22}$$

i.e., in the simple pendulum case we get (12) with $c = 1$ and $c = 0$, respectively.

3.4. Implicit midpoint rule

Any first-order equation, $\dot{x} = F(x)$, can be discretized using the implicit midpoint rule (which coincides with the implicit one-stage Gauss–Legendre–Runge–Kutta method; compare [11]). The first derivative is replaced by the difference quotient and the right-hand side is evaluated at the midpoint $\frac{1}{2}(x_n + x_{n+1})$. In the case of the simplest Hamiltonian systems, given by (2), we have

$$\varphi_{k+1} = \varphi_k + \frac{1}{2}\varepsilon(p_k + p_{k+1}), \qquad p_{k+1} = p_k + \varepsilon f\left(\frac{\varphi_k + \varphi_{k+1}}{2}\right). \tag{23}$$

In the special case of the simple pendulum, we get

$$\begin{aligned} &\frac{\varphi_{k+1} - 2\varphi_k + \varphi_{k-1}}{\varepsilon^2} = -\frac{1}{2}k\left(\sin\left(\frac{\varphi_{k+1} + \varphi_k}{2}\right) + \sin\left(\frac{\varphi_k + \varphi_{k-1}}{2}\right)\right), \\ &p_k = \frac{\varphi_{k+1} - \varphi_k}{\varepsilon} + \frac{1}{2}\varepsilon k \sin\frac{\varphi_{k+1} + \varphi_k}{2}. \end{aligned} \tag{24}$$

The implicit midpoint rule has quite good properties: this is a symplectic, time-reversible method of order 2. The symplecticity follows directly from lemma 1. Indeed, (23) implies $P_{,1} = P_{,2}$ and $R_{,1} = R_{,2}$.

4. Projection methods

Non-integrable discretizations can be modified so as to preserve the energy integral 'by force', i.e., projecting the result of every step on the constant energy manifold. In principle, any one-step method can be converted into the corresponding projection method. In this paper, we apply these procedures to the Störmer–Verlet (leap-frog) method. Therefore, referring to the 'standard projection' and 'symmetric projection' we always mean the standard (or symmetric) projection applied to the leap-frog scheme.

4.1. The standard projection method

There are given a first-order equation $\dot{x} = F(x), x \in \mathbb{R}^2$, any one-step numerical method $x_{n+1} = \Phi_\varepsilon(x_n)$ (a discretization of the ODE) and a constraint $g(x) = 0$ that we would like to preserve. The standard projection consists in computing $\tilde{x}_{n+1} := \Phi_\varepsilon(x_n)$, and then orthogonally projecting $\tilde{x}_{n+1}$ on the manifold $g(x) = 0$; see [11]. This projection, denoted by x_{n+1}, yields the next step: $x_n \to x_{n+1}$. In other words, we define

$$x_{n+1} = \tilde{x}_{n+1} + \lambda \nabla g(\tilde{x}_{n+1}) \tag{25}$$

where λ is such that $g(x_{n+1}) = 0$.

Applying this approach to the simple pendulum (5) it is convenient to define x as

$$x = \left(\varphi, \frac{\dot{\varphi}}{\omega}\right) \equiv (\varphi, p), \tag{26}$$

where $\omega = \sqrt{k}$. The above definition of p yields dimensionless components of x. If $k = 1$ (which is assumed throughout this paper), then this definition of p coincides with the previous one; see (2). The constraint $g(x) = 0$ is given by (6), i.e.,

$$g(x) = \tfrac{1}{2}p^2 - \cos\varphi - h, \tag{27}$$

where $h = E/\omega^2$. Equation (25) becomes

$$\varphi_{n+1} = \tilde{\varphi}_{n+1} + \lambda \sin\tilde{\varphi}_{n+1}, \qquad p_{n+1} = (1+\lambda)\tilde{p}_{n+1}, \tag{28}$$

and λ is computed from

$$\tfrac{1}{2}(1+\lambda)^2\tilde{p}_{n+1}^2 - \cos(\tilde{\varphi}_n + \lambda\sin\tilde{\varphi}_{n+1}) = h. \tag{29}$$

In order to solve (29) we use Newton's iteration $\lambda_{j+1} = \lambda_j + \Delta\lambda_j$, where

$$\Delta\lambda_j = -\frac{\frac{1}{2}(1+\lambda_j)^2\tilde{p}_{n+1}^2 - \cos(\tilde{\varphi}_n + \lambda_j\sin\tilde{\varphi}_{n+1}) - h}{\tilde{p}_{n+1}^2 + \sin^2\tilde{\varphi}_{n+1}}, \tag{30}$$

and it is sufficient and convenient to choose $\lambda_0 = 0$. The approximated solution to (29) is given by $\lambda = \lim_{j\to\infty}\lambda_j$.

4.2. The symmetric projection method

A one-step algorithm $x_{n+1} = \Phi_\varepsilon(x_n)$ is called symmetric (or time-reversible) if $\Phi_{-\varepsilon} = \Phi_\varepsilon^{-1}$. Equations of the classical mechanics are time reversible; therefore, the preservation of this property is convenient and is expected to improve numerical results. The symplectic Euler methods are not time reversible while the Störmer–Verlet method and implicit midpoint rule are symmetric. The symmetry can be easily noted in the form (13) of the leap-frog method.

The symmetric projection method preserves the time reversibility. The method is applied under similar assumptions as standard projection (additionally we demand the time reversibility of Φ_ε) and consists of the following steps [2, 10]:

$$\hat{x}_n = x_n + \lambda\nabla g(x_n), \qquad \tilde{x}_{n+1} = \Phi_\varepsilon(\hat{x}_n), \qquad x_{n+1} = \tilde{x}_{n+1} + \lambda\nabla g(\tilde{x}_{n+1}), \tag{31}$$

where we assume $g(x_n) = 0$ and compute the parameter λ from the condition $g(x_{n+1}) = 0$.

5. Integrable discretizations

Throughout this paper by integrability we mean the existence of an integral of motion. The Newton equation (1) has the energy integral (3). Its discretization is called integrable when it has an integral of motion as well. In the continuum limit this integral becomes the energy integral, so it may be treated as a discrete analogue of the energy.

5.1. Standard-like discretizations

Standard-like discretizations are defined by [26]

$$\varphi_{n+1} = \varphi_n + \varepsilon p_{n+1}, \qquad p_{n+1} = p_n + \varepsilon F(\varphi_n, \varepsilon), \tag{32}$$

where F has to satisfy $F(\varphi_n, 0) = f(\varphi_n)$. For a given f there exist infinitely many functions F satisfying this conditions. All of them are symplectic, which can be easily seen applying lemma 1 with $P_{,1} = R_{,2} = 0$. Similarly as in section 3 we obtain from (32)

$$\begin{aligned} &\varphi_{n+1} - 2\varphi_n + \varphi_{n-1} = \varepsilon^2 F(\varphi_n, \varepsilon), \\ &p_n = \frac{\varphi_{n+1} - \varphi_n}{\varepsilon} - \varepsilon F(\varphi_n, \varepsilon) = \frac{\varphi_n - \varphi_{n-1}}{\varepsilon}. \end{aligned} \tag{33}$$

We are interested in integrable cases, i.e., in discretizations preserving the energy integral. Suris found that two standard-like discretizations of the simple pendulum are integrable [25, 26]:

$$\varphi_{n+1} - 2\varphi_n + \varphi_{n-1} = -2\arctan\left(\frac{k\varepsilon^2 \sin\varphi_n}{2 + k\varepsilon^2\cos\varphi_n}\right), \tag{34}$$

$$\varphi_{n+1} - 2\varphi_n + \varphi_{n-1} = -4\arctan\left(\frac{k\varepsilon^2 \sin\varphi_n}{4 + k\varepsilon^2\cos\varphi_n}\right). \tag{35}$$

Equation (34), referred to as the Suris1 scheme, has the integral of motion given by

$$E_1 = \frac{1}{2}\left(\frac{2\sin\frac{\varphi_{n+1}-\varphi_n}{2}}{\varepsilon}\right)^2 - \frac{1}{2}k(\cos\varphi_n + \cos\varphi_{n+1}), \tag{36}$$

or, in terms of φ_n and p_n,

$$E_1 = \frac{1-\cos\varepsilon p_n}{\varepsilon^2} - \frac{1}{2}k(\cos\varphi_n + \cos(\varphi_n - \varepsilon p_n)). \tag{37}$$

Equation (35), referred to as the Suris2 scheme, has the following integral of motion:

$$E_2 = \frac{1}{2}\left(\frac{4\sin\frac{\varphi_{n+1}-\varphi_n}{4}}{\varepsilon}\right)^2 - k\cos\frac{\varphi_n + \varphi_{n+1}}{2}, \tag{38}$$

which can be expressed in terms of φ_n and p_n as follows:

$$E_2 = \frac{4}{\varepsilon^2}\left(1 - \cos\frac{\varepsilon p_n}{2}\right) - k\cos\left(\varphi_n - \frac{\varepsilon p_n}{2}\right). \tag{39}$$

One can verify the preservation of these integrals by direct computation.

5.2. The discrete gradient method

The discrete gradient method [21–23] is a general and very powerful method to generate numerical schemes preserving any number of integrals of motion and some other properties [20]. However, this method, in general, is not symplectic. In this paper, we need to preserve one integral (the energy) and the system is Hamiltonian, compare (4),

$$\dot\varphi = \frac{\partial H}{\partial p}, \qquad \dot p = -\frac{\partial H}{\partial \varphi}. \tag{40}$$

In such a case, the discrete gradient method reduces to the following simple scheme. Left-hand sides of formulae (40) are discretized in the simplest way (difference quotients) while the right-hand sides are replaced by the so-called discrete (or average) gradients:

$$\frac{\varphi_{n+1} - \varphi_n}{\varepsilon} = \frac{\Delta H}{\Delta p}, \qquad \frac{p_{n+1} - p_n}{\varepsilon} = -\frac{\Delta H}{\Delta \varphi}. \tag{41}$$

The discrete gradient $\bar\nabla H \equiv \left(\frac{\Delta H}{\Delta\varphi}, \frac{\Delta H}{\Delta p}\right)$ of a differentiable function $H(\varphi, p)$ by definition (see [21]) satisfies the condition

$$H(\varphi_{n+1}, p_{n+1}) - H(\varphi_n, p_n) = \frac{\Delta H}{\Delta\varphi}(\varphi_{n+1} - \varphi_n) + \frac{\Delta H}{\Delta p}(p_{n+1} - p_n). \tag{42}$$

The explicit form of $\bar\nabla H$ is, in general, not unique. One of the possibilities is the coordinate increment discrete gradient [15],

$$\frac{\Delta H}{\Delta\varphi} = \frac{H(\varphi_{n+1}, p_n) - H(\varphi_n, p_n)}{\varphi_{n+1} - \varphi_n}, \qquad \frac{\Delta H}{\Delta p} = \frac{H(\varphi_{n+1}, p_{n+1}) - H(\varphi_{n+1}, p_n)}{p_{n+1} - p_n}. \tag{43}$$

Other possibilities are, for instance, mean value discrete gradient [21] and midpoint discrete gradient [8]. All these definitions coincide in the case $H(\varphi, p) = T(p) + V(\varphi)$. In such a case $\bar{\nabla} H = (\bar{\nabla} V, \bar{\nabla} T)$, where

$$\bar{\nabla} T = \frac{T(p_{n+1}) - T(p_n)}{p_{n+1} - p_n}, \qquad \bar{\nabla} V = \frac{V(\varphi_{n+1}) - V(\varphi_n)}{\varphi_{n+1} - \varphi_n}. \tag{44}$$

Thus we have got the discrete gradient scheme:

$$\begin{cases} \dfrac{p_{n+1} + p_n}{2} = \dfrac{\varphi_{n+1} - \varphi_n}{\varepsilon}, \\ \dfrac{p_{n+1} - p_n}{\varepsilon} = -\dfrac{V(\varphi_{n+1}) - V(\varphi_n)}{\varphi_{n+1} - \varphi_n}. \end{cases} \tag{45}$$

This numerical scheme can also be obtained as a special case of the modified midpoint rule [16]. The system (45) can be rewritten as the following second-order equation for φ_n plus the defining equation for p_n:

$$\begin{aligned} \frac{\varphi_{n+1} - 2\varphi_n + \varphi_{n-1}}{\varepsilon^2} &= -\frac{1}{2}\left(\frac{V(\varphi_{n+1}) - V(\varphi_n)}{\varphi_{n+1} - \varphi_n} + \frac{V(\varphi_n) - V(\varphi_{n-1})}{\varphi_n - \varphi_{n-1}} \right) \\ p_n &= \frac{\varphi_{n+1} - \varphi_n}{\varepsilon} + \frac{1}{2}\varepsilon \left(\frac{V(\varphi_{n+1}) - V(\varphi_n)}{\varphi_{n+1} - \varphi_n} \right). \end{aligned} \tag{46}$$

Substituting $V(\varphi) = -k\cos\varphi$ we get the simple pendulum case. Multiplying both equations (45) side by side, we easily prove that the system (46) has the first integral

$$E = \tfrac{1}{2} p_n^2 + V(\varphi_n) \tag{47}$$

which exactly coincides with the Hamiltonian (4) evaluated at φ_n, p_n. Note that the integrals of motion (37), (39) coincide with (4) (where $V(\varphi) = -k\cos\varphi$) only approximately in the limit $\varepsilon \to 0$.

6. A correction which preserves the period of small oscillations

The classical harmonic oscillator equation $\ddot{\varphi} + \omega^2 \varphi = 0$ admits the exact discretization ([6], compare also [1, 24]), i.e., a discretization such that the solution $\varphi(t)$ evaluated at $n\varepsilon$ equals φ_n (for any ε and any n):

$$\varphi_{n+1} - 2\varphi_n \cos\varepsilon\omega + \varphi_{n-1} = 0, \qquad p_n = \frac{\omega}{\sin\omega\varepsilon}(\varphi_{n+1} - \varphi_n \cos\omega\varepsilon). \tag{48}$$

The energy is also exactly preserved, i.e.,

$$E = \tfrac{1}{2} p_n^2 + \tfrac{1}{2}\omega^2 \varphi_n^2 \tag{49}$$

does not depend on n (which can easily be checked by direct calculation). The existence of the exact discretization of the harmonic oscillator equation has been recently used to discretize the Kepler problem (preserving all integrals of motion and trajectories) [5].

We consider the class of Newton equations (1). Let us confine ourselves to equations which have a stable equilibrium at $\varphi = 0$, i.e., $f'(0) < 0$. Then $V = V(\varphi)$ has a local minimum at $\varphi = 0$, i.e., $V'(0) = f(0) = 0$. We denote

$$\omega_0 = \sqrt{V''(0)}. \tag{50}$$

Thus

$$V(\varphi) = V_0 + \tfrac{1}{2}\omega_0^2 \varphi^2 + \cdots, \tag{51}$$

and small oscillations around the equilibrium can be approximated by the classical harmonic oscillator equation with $\omega = \omega_0$.

Do exist discretizations which in the limit $\varphi_n \approx 0$ (ε is fixed) become exact? Known discretizations, including those presented in this paper, do not have this property. Fortunately, we found such a discretization by modifying the discrete gradient method. It is sufficient to replace ε by some function $\delta = \delta(\varepsilon)$ in formulae (45). The form of this function will be obtained by the comparison with the harmonic oscillator equation (in the limit $\varphi \approx 0$).

We linearize equations (46) (with ε replaced by δ) around $\varphi_n = 0$ (i.e., we take into account (51)). Thus we get

$$\begin{aligned} &\frac{\varphi_{n+1} - 2\varphi_n + \varphi_{n-1}}{\delta^2} = -\frac{\omega_0^2}{4}\left(\varphi_{n+1} + 2\varphi_n + \varphi_{n-1}\right), \\ &p_n = \frac{\varphi_{n+1} - \varphi_n}{\delta} + \frac{1}{4}\omega_0^2\delta(\varphi_{n+1} + \varphi_n), \end{aligned} \tag{52}$$

which is equivalent to

$$\begin{aligned} &\varphi_{n+1} - 2\left(\frac{4 - \omega_0^2\delta^2}{4 + \omega_0^2\delta^2}\right)\varphi_n + \varphi_{n-1} = 0, \\ &p_n = \frac{4 + \omega_0^2\delta^2}{4\delta}\left(\varphi_{n+1} - \left(\frac{4 - \omega_0^2\delta^2}{4 + \omega_0^2\delta^2}\right)\varphi_n\right). \end{aligned} \tag{53}$$

We compare (48) with (53). Both systems coincide if and only if

$$\frac{4 - \omega_0^2\delta^2}{4 + \omega_0^2\delta^2} = \cos\varepsilon\omega, \qquad \frac{4 + \omega_0^2\delta^2}{4\delta} = \frac{\omega}{\sin\varepsilon\omega}. \tag{54}$$

Solving the system (54) we get

$$\omega = \omega_0, \qquad \delta = \frac{2}{\omega_0}\tan\left(\frac{\varepsilon\omega_0}{2}\right). \tag{55}$$

Therefore, we propose the following new discretization of the Newton equations (1), (3) (modified discrete gradient scheme):

$$\begin{aligned} &\frac{\varphi_{n+1} - 2\varphi_n + \varphi_{n-1}}{\delta^2} = -\frac{1}{2}\left(\frac{V(\varphi_{n+1}) - V(\varphi_n)}{\varphi_{n+1} - \varphi_n} + \frac{V(\varphi_n) - V(\varphi_{n-1})}{\varphi_n - \varphi_{n-1}}\right) \\ &p_n = \frac{\varphi_{n+1} - \varphi_n}{\delta} + \frac{1}{2}\delta\left(\frac{V(\varphi_{n+1}) - V(\varphi_n)}{\varphi_{n+1} - \varphi_n}\right), \end{aligned} \tag{56}$$

where δ is defined by (55) (and ω_0 is given by (50)). This discretization becomes exact for small oscillations for any fixed ε. It means that for $\varphi_n \approx 0$ the period and the amplitude of the approximated solution should be very close to the exact values (even for large ε!). In the following sections we will verify this point experimentally.

7. Numerical experiments

We performed a number of numerical experiments applying the numerical schemes presented above. The initial data were parametrized by the velocity p_0 while the initial position was always the same: $\varphi_0 = 0$. In the continuous case (5) we have three possibilities: oscillating motion ($|p_0| < 2$), rotating motion ($|p_0| > 2$) and the motion along the separatrix ($p_0 = \pm 2$), from $\varphi = 0$ to (asymptotically) $\varphi = \pm\pi$. The (theoretical) amplitude A_{th} for the oscillating

motions can easily be computed from the energy conservation law (6) (where $k = 1$, i.e., $\frac{1}{2}p_0^2 - 1 = -\cos A_{\text{th}}$):

$$2 \sin \frac{A_{\text{th}}}{2} = p_0. \tag{57}$$

In particular, we performed many numerical computations for the following initial data:

- $p_0 = 0.1$, then $A_{\text{th}} \approx 0.031\,8443\pi \approx 0.100\,0417$ (small amplitude)
- $p_0 = 1.8$, then $A_{\text{th}} \approx 0.712\,867\pi \approx 2.239\,539$ (very large amplitude).

To estimate the actual amplitude of a given discrete simulation we apply the following procedure: if φ_m is a local maximum of the discrete trajectory (i.e., $\varphi_m > \varphi_{m-1}$ and $\varphi_m > \varphi_{m+1}$), then we estimate the maximum of the approximated function by the maximum of the parabola best fitted to the following five points: $\varphi_{m-2}, \varphi_{m-1}, \varphi_m, \varphi_{m+1}, \varphi_{m+2}$. The analogical procedure is done also at local minima (we take the absolute value of the obtained minimum). Thus we obtain a sequence of the amplitudes, A_N. The index N is common for all extrema (maxima and minima), and on some figures we denote it by $N_{1/2}$ (the number of half periods) to discern it from N (the number of periods).

Every numerical scheme used in the present paper yields a discrete trajectory with a rather stable amplitude. It is not constant but oscillates in a regular way around an average value:

$$A_N = A(1 + \alpha_N), \tag{58}$$

where both the average amplitude A and relative (dimensionless) oscillations α_N can depend on the time step ε and on the initial velocity p_0, i.e., $A = A(p_0, \varepsilon)$ and $\alpha_N = \alpha_N(p_0, \varepsilon)$. Of course, both A and α_N differ for different numerical schemes.

In a similar way, we estimated the period of discrete motions. The exact periodicity ($\varphi_{k+n} = \varphi_k$ for some k, n) is a rare phenomenon and, of course, we did not observe it. To define the approximate period we fit a continuous curve to the discrete graph, estimate zeros of this function, and compute the distance between the neighbouring zeros.

Suppose that $\varphi_m \varphi_{m+1} < 0$ for some m. It means that one of the zeros, say z_N, lays between φ_m and φ_{m+1}. We estimate it by zero of the interpolating cubic polynomial based on the points $\varphi_{m-1}, \varphi_m, \varphi_{m+1}, \varphi_{m+2}$ (another natural, but less accurate, possibility could be a line joining φ_m and φ_{m+1}). Then, denoting subsequent estimated zeros by z_N ($N = 1, 2, 3, \ldots$) and $z_0 = \varphi_0 = 0$, we define

$$T_N = z_{2N} - z_{2N-2}, \tag{59}$$

which we take as an estimate of the period.

Our numerical experiments have shown that T_N is not exactly constant but oscillates with a relatively small amplitude. The average value of T_N is constant with high accuracy (see the following section). Therefore we have

$$T_N = T(1 + \tau_N), \tag{60}$$

where both the average period T and relative (dimensionless) oscillations τ_N can depend on the time step ε and on the initial velocity p_0, i.e., $T = T(p_0, \varepsilon)$ and $\tau_N = \tau_N(p_0, \varepsilon)$. Moreover, T and τ_N essentially depend on the discretization (numerical scheme).

The amplitude of small oscillations is defined in a natural way:

$$\tau(\varepsilon, p_0) := \max_N |\tau_N(\varepsilon, p_0)|, \qquad \alpha(\varepsilon, p_0) := \max_N |\alpha_N(\varepsilon, p_0). \tag{61}$$

Fortunately, $|\tau_N|$ and $|\alpha_N|$ oscillate (as functions of N), with small amplitudes, in a very regular way. Thus we can estimate $\tau(\varepsilon, p_0)$ and $\alpha(\varepsilon, p_0)$ considering a series of, say, 40 local extrema of τ_N and α_N, and taking an average value.

8. Periodicity and stability

Discrete trajectories generated by symplectic or integrable schemes considered in our paper are stable for ε which are not too large (for very large ε one can observe chaotic behaviour [7, 29]). We confine ourselves to sufficiently small ε, i.e. $\varepsilon \leqslant 0.5$, but sometimes (for $p_0 < 1.5$) we can take even $\varepsilon \approx 1$. In this region the motion is very stable, and both the average period T and the average amplitude A are well defined. The average amplitude is computed simply as

$$A_{\mathrm{avg}}(N, M) = \frac{1}{M} \sum_{j=0}^{M-1} |A_{N+j}|, \tag{62}$$

where we usually assume $M = 50$. The definition of the average period is similar. In many cases we use the formula

$$T_{\mathrm{avg}}(N, M) = \frac{1}{M}(z_{N+2M} - z_N), \tag{63}$$

where the dependence (very essential!) on ε and p_0 is omitted for the sake of brevity. Note that $T_N \equiv T_{\mathrm{avg}}(2N-2, 1)$. Computing T_{avg} it is necessary to choose M arbitrarily, we usually take $M = 20$. Sometimes we denote $N \equiv N_0$ to point out that the average is taken over indices greater than N_0.

Considering very long discrete evolutions (many thousands of periods), we use another definition of the average period. Namely, we average $T_{\mathrm{avg}}(N, M)$ over some range of the parameter M ($K < M \leqslant L$):

$$\bar{T}_{\mathrm{avg}}(N, K, L) = \frac{1}{L-K} \sum_{M=K+1}^{L} T_{\mathrm{avg}}(N, M). \tag{64}$$

Usually we assume $K = 100$, $L = 200$.

All discretizations considered in the present paper are characterized by very high stability of the period and the amplitude. One can hardly notice any dependence of T_{avg} and A_{avg} on N, even when testing very large N (such as 10^3, 10^5 or 10^6), and $\bar{T}_{\mathrm{avg}}$ is even more stable.

As a typical example we present long-time behaviour of the Suris1 scheme; see figures 1 and 2, where we used the definition (63) with $M = 20$. The time dependence of the average period yields an interesting periodic pattern (one can discern distinct 'discrete curves'). The origin of such patterns is explained in section 9. An interesting phenomenon is associated with changing M. The patterns for different M usually are very similar but the amplitude of oscillations becomes smaller and smaller for larger M (compare figure 3, where $M = 1$, with figure 2, where $M = 20$).

Table 1 shows how stable are the periods of the oscillations. Maximal T_N is defined as $\max_{J+100<N\leqslant J+200} T_N$ for either $J = 0$ or $J = 1.8 \times 10^6$. Minimal values and the average are taken over the same range of values. The standard error of the average is about 5.7×10^{-8} (the maximal error is about 10^{-7}). Therefore, the average period is practically constant for all studied discretizations. The Suris1 scheme is exceptionally stable. In this case, any variations of the period are well within the error limits, and we did not observe any dependence of $T_{\mathrm{avg}}(N, M)$ on N. Taking into account the observed stability of the period, throughout this paper we identify the average period with $T \equiv T_{\mathrm{avg}}(0, 20)$.

The observed stability of the period (for symplectic and integrable discretizations) is in sharp contrast to the results given by standard (non-symplectic and non-integrable) numerical methods. For instance, the most popular (explicit) fourth-order Runge–Kutta scheme yields the period noticeably decreasing in time (see figure 4). For small N_0 we get reasonably good

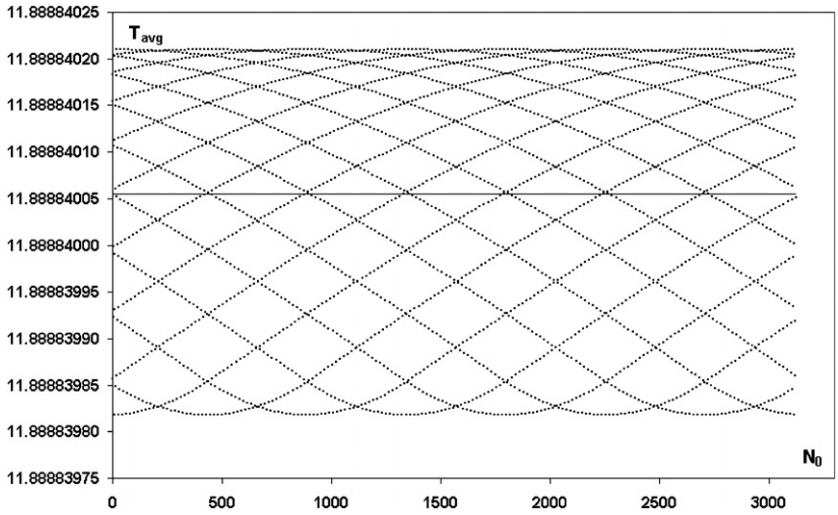

Figure 1. $T_{\mathrm{avg}}(N_0, 20)$ for the Suris1 scheme ($N_0 < 3100$), $\varepsilon = 0.2$, $p_0 = 1.95$, $T_{\mathrm{th}} = 11.657\,585\,28$, $T = 11.888\,840\,05$.

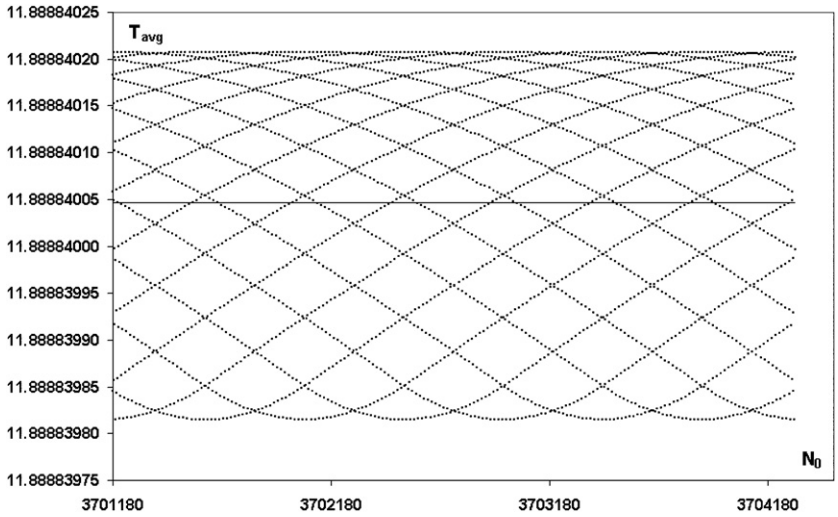

Figure 2. $T_{\mathrm{avg}}(N_0, 20)$ for the Suris1 scheme (for very large N_0), $\varepsilon = 0.2$, $p_0 = 1.95$, $T_{\mathrm{th}} = 11.657\,585\,28$, $T = 11.888\,840\,05$.

estimation of the period (interpolating the discrete curve we get $T = 11.646\,02$ for $N_0 = 0$, which is quite close to the theoretical value $T_{\mathrm{th}} = 11.657\,585\,28$). Among our discretizations only both gradient schemes produce comparable (even a little bit better) results, namely the discrete gradient scheme yields $T = 11.646\,98$. However, for larger N_0 the Runge–Kutta method yields worse and worse estimation of the period (in fact, this is an exponential decrease, although very slow) while both gradient methods remain stable for very long time; compare table 1. In this particular case ($p_0 = 1.95$, $\varepsilon = 0.2$), the error produced by the Runge–Kutta

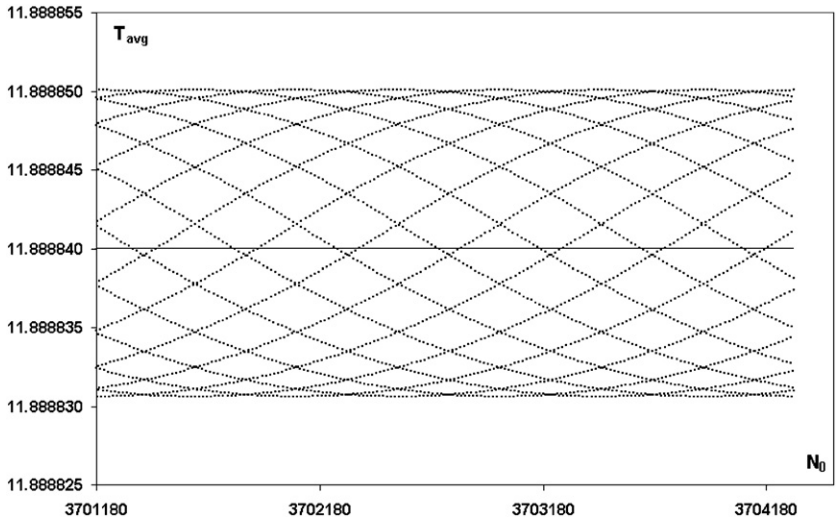

Figure 3. T_N for the Suris1 scheme (for very large N), $\varepsilon = 0.2$, $p_0 = 1.95$, $T_{\text{th}} = 11.657\,585\,28$, $T = 11.888\,840\,05$.

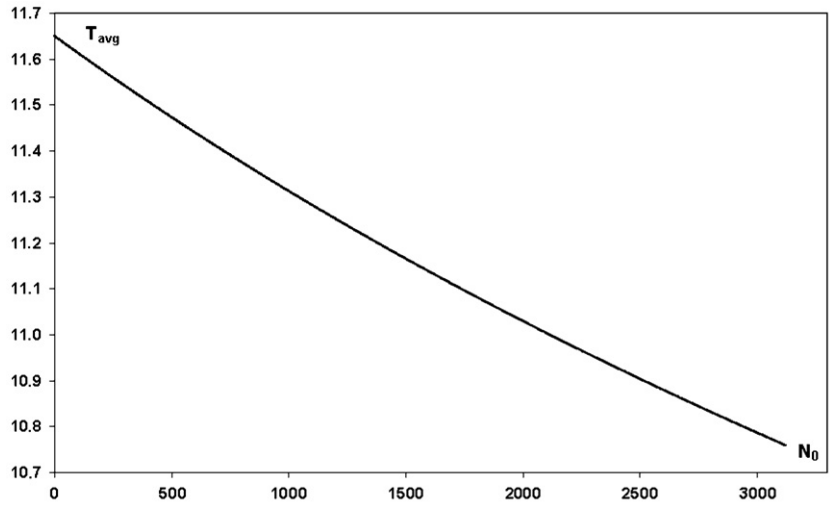

Figure 4. $T_{\text{avg}}(N_0, 20)$ for a fourth-order Runge-Kutta scheme, $\varepsilon = 0.2$, $p_0 = 1.95$, $T_{\text{th}} = 11.657\,585\,28$.

method becomes greater than the errors of all methods considered in this paper beginning from $N_0 \approx 2000$.

Numerical experiments show that the oscillations of the period and the amplitude are very small. For $\varepsilon \to 0$ we have $\tau(\varepsilon, p_0) \to 0$, up to the round-off error. The largest values of $\tau(\varepsilon, p_0)$, obtained for both projection methods (for large ε and small p_0), are of order 0.2. All other discretizations yield oscillations smaller by one or two orders of magnitude (even for large ε). A typical picture is given in figure 5 representing $\tau(\varepsilon, p_0)$ for $p_0 = 1.8$.

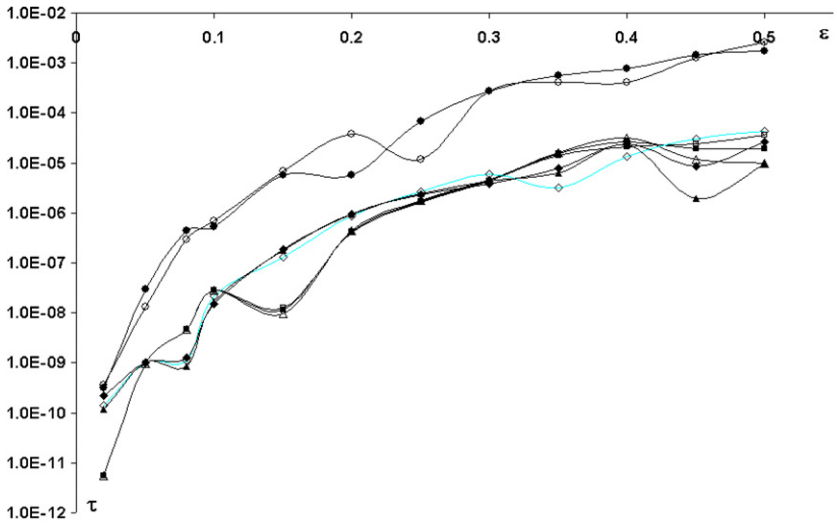

Figure 5. Relative amplitude of the period oscillations (τ) for $p_0 = 1.8$. The vertical axis is marked with a logarithmic scale. Black circles: symmetric projection, white circles: standard projection, black squares: Suris2 (Suris1 and leap-frog yield almost the same values), black triangles: implicit midpoint, black diamonds: modified discrete gradient, white diamonds: discrete gradient (the last three methods yields similar values, especially for $0.1 < \varepsilon < 0.3$).

Table 1. Stability of the period. Minimal, maximal and average values of T_N for $p_0 = 1.95$, $\varepsilon = 0.2$ ($T_{\text{th}} = 11.657\,585\,28$).

		Leap-frog	Suris1	Discrete gradient
Maximal T_N	$N < 100$	11.931 660 41	11.888 850 08	11.646 985 00
	$N \approx 1.8 \times 10^6$	11.931 660 40	11.888 850 08	11.646 985 40
Minimal T_N	$N < 100$	11.931 641 45	11.888 830 61	11.646 971 57
	$N \approx 1.8 \times 10^6$	11.931 641 40	11.888 830 61	11.646 971 90
Average:	$N = 0$	11.931 651 74	11.888 840 05	11.646 977 32
$\tilde{T}_{\text{avg}}(N, 100, 200)$	$N = 1.8 \times 10^6$	11.931 651 62	11.888 840 01	11.646 977 64

9. Why do the period and the amplitude oscillate in a very regular way?

In a large range of parameters, the oscillations τ_N are very regular and their amplitude is greater than numerical errors by several orders of magnitude. This phenomenon turns out to be mainly caused by systematic numerical by-effects.

Our explanation is associated with the above procedure of estimating zeros. In general, the period $T \equiv T_{\text{avg}}$ and ε is incommensurable. Therefore, the relative position of z_N between φ_m and φ_{m+1} depends on N. We conjecture that the periodic phenomena one observes at figures 6–11 are associated with the properties of the real number T/ε, namely, with the approximation of T/ε and $T/(2\varepsilon)$ by rational numbers.

We begin with a simple definitions. Given $T, \varepsilon \in \mathbb{R}$ ($T > \varepsilon > 0$) and $K \in \mathbb{N}$ we define

$$\mu_K := \frac{KT}{\varepsilon} - M_K, \qquad \nu_K := \frac{KT}{2\varepsilon} - L_K, \tag{65}$$

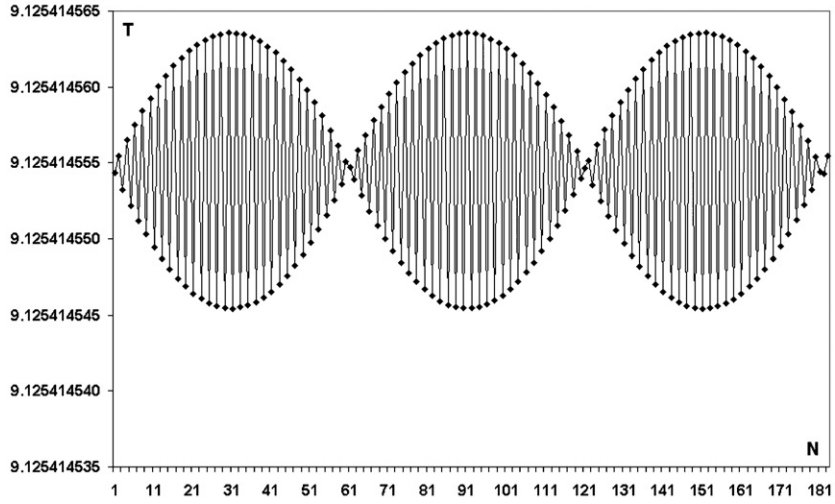

Figure 6. T_N for the leap-frog scheme, $\varepsilon = 0.05$, $p_0 = 1.8$, $T = 9.125\,414\,5545$.

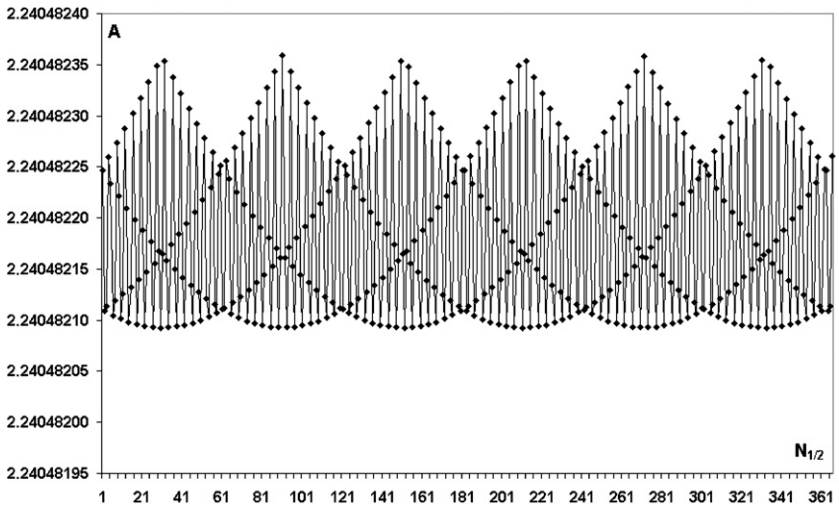

Figure 7. A_N for the leap-frog scheme, $\varepsilon = 0.05$, $p_0 = 1.8$, $T = 9.125\,414\,5545$.

such that $-0.5 < \mu_K \leqslant 0.5$, $-0.5 < \nu_K \leqslant 0.5$ and $M_K, L_K \in \mathbb{N}$. In other words, for a given K we take M_K such that M_K/K is the best rational approximation (with a given denominator K) of the real number T/ε, and L_K/K is the best rational approximation (with the denominator K) of $T/(2\varepsilon)$. For given T, ε, K formulae (65) define uniquely μ_K, ν_K, M_K, L_K. The following lemma can be derived directly from the above definitions.

Lemma 3. *Suppose that $T > \varepsilon > 0$ are given:*

(i) If $|\mu_K + \mu_J| < 0.5$, then $M_{K+J} = M_K + M_J$ and $\mu_{K+J} = \mu_K + \mu_J$.
(ii) If $|\nu_K + \nu_J| < 0.5$, then $L_{K+J} = L_K + L_J$ and $\nu_{K+J} = \nu_K + \nu_J$.
(iii) If $|\nu_K| < 0.25$, then $M_K = 2L_K$ and $\mu_K = 2\nu_K$.

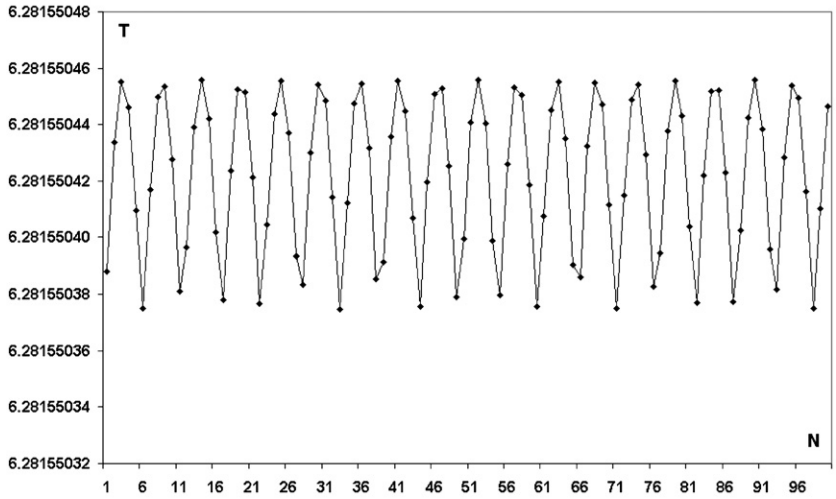

Figure 8. T_N for the leap-frog scheme, $\varepsilon = 0.1$, $p_0 = 0.05$, $T = 6.281\,550\,4224$.

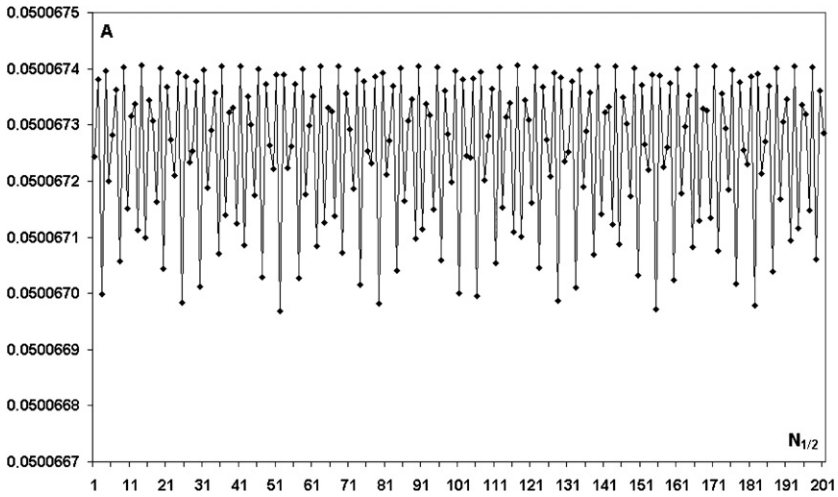

Figure 9. A_N for the leap-frog scheme, $\varepsilon = 0.1$, $p_0 = 0.05$, $T = 6.281\,550\,4224$.

(iv) If K is even, then $M_{K/2} = L_K$ and $\mu_{K/2} = \nu_K$.

Corollary 1. *If $\nu_K \approx 0$, then $\mu_K \approx 0$ and, for K even, also $\mu_{K/2} \approx 0$.*

If $\mu_K \approx 0$, then the configuration of z_N, φ_m, φ_{m+1} practically repeats after every K periods. Therefore, it is natural to expect some periodic recurrences with the period KT. In particular, $\tau_{N+K} \approx \tau_N$ for any N.

To obtain a 'good' approximation we usually demand at least $\mu_K < 0.01$. Sometimes, especially for small K (e.g., $K \leqslant 5$), interesting effects can be observed also for larger μ_K (but, anyway, $\mu_K < 0.1$): the graph of the function $N \to T_N$ apparently splits into K 'discrete curves' (T_N and T_M belong to the same curve if $N = M \pmod K$).

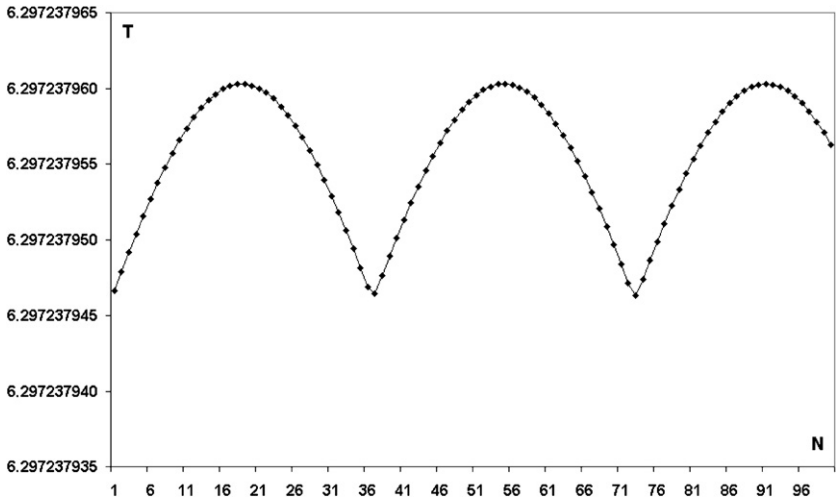

Figure 10. T_N for the Suris1 scheme, $\varepsilon = 0.1$, $p_0 = 0.05$, $T = 6.297\,237\,955$.

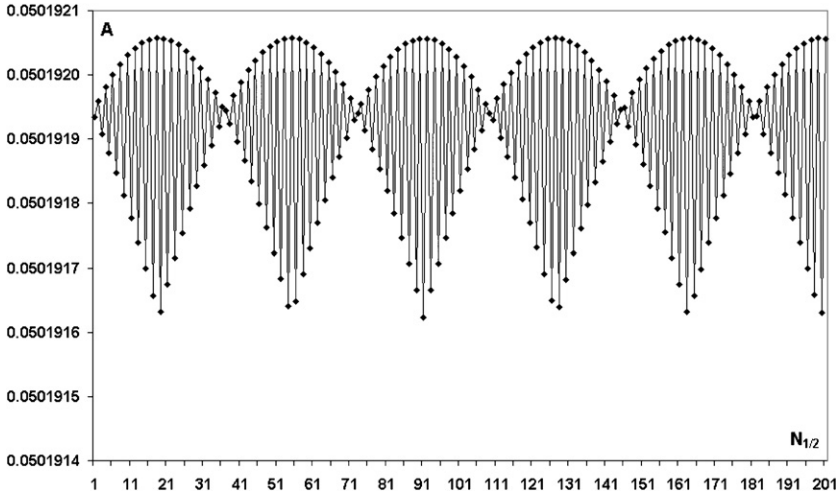

Figure 11. A_N for the Suris1 scheme, $\varepsilon = 0.1$, $p_0 = 0.05$, $T = 6.297\,237\,955$.

Similar considerations can be made for the oscillations α_N of the amplitude. In this case the period is $T/2$, and 'good' approximations correspond to $\nu_K \approx 0$.

Example 1 (leap-frog scheme, $\varepsilon = 0.05$, $p_0 = 1.8$, $T \approx 9.125\,4146$)**.** We compute $T/\varepsilon \approx 182.508\,291$ and easily check that $\mu_2 \approx 0.017$, $\mu_{59} \approx -0.011$, $\mu_{61} \approx 0.0058$, $\mu_{120} \approx -0.0051$, $\mu_{181} \approx 0.000\,67$. Figure 6 confirms that the characteristic 'time scales' responsible for the pattern of the oscillations are 2, 120 and 181 indeed.

The period 2 corresponds to oscillations between two sinusoid-like curves. Namely, T_N belong to the first 'sinusoid' for N odd, and to second 'sinusoid' for N even. Both discrete curves are periodic with the period 120. Actually, the whole picture seems to have the translational symmetry with the period 60. The difference between T_{N+60} and T_N is quite large (in this sense 60 is not a period, indeed); however, T_N lays between T_{N+59} and T_{N+61}.

The next period, 181, is more difficult to be noticed and corresponds to more subtle effects, such as the configuration of points near intersections of both 'sinusoids' which approximately repeats every three 'sinusoid' half periods.

Similarly, we compute $\nu_4 \approx 0.017$, $\nu_{59} \approx -0.0054$, $\nu_{181} \approx 0.000\,34$ and $\nu_{240} \approx -0.0051$. In figure 7, we recognize four discrete curves, periodic with the period 240. The whole picture has the period 60 but looking closely on some details (e.g., at peaks or at intersections) we can also notice another periodicity with the period 181.

Finally, we point out that all equalities suggested by lemma 3 hold (e.g., $\mu_{61} = \mu_2 + \mu_{59}$, $\nu_{240} = \nu_{59} + \nu_{181}$, $\mu_{59} = 2\nu_{59}$, $\mu_4 = \nu_2$, etc).

Example 2 (leap-frog scheme, $\varepsilon = 0.1$, $p_0 = 0.05$, $T \approx 6.281\,550\,42$)**.** $T/\varepsilon \approx 62.815\,504$ and we check that $\mu_5 = 0.078$, $\mu_{11} = -0.029$, $\mu_{27} = 0.019$, $\mu_{38} = -0.011$, $\mu_{65} = 0.0078$, $\mu_{103} = -0.0031$. Figure 8 does not look so regularly as figure 6. Note that μ_K are now relatively large; the first μ_K smaller than 0.01 has the index $K = 65$ and the next one is $K = 103$. However, a closer inspection reveals similar features in both figures. We have five sinusoid-like curves (periodic with the period 65). The distance between them is 13 but the difference between T_{N+13} and T_N is large. Note that the period $103 \approx 8 \times 13$, so points of only every eighth 'sinusoid' practically coincide.

The other periods ($K = 11, 27, 38$) can be derived from 103 and 65, namely: $38 = 103 - 65, 27 = 65 - 38, 11 = 38 - 27$. They can be noticed in figure 8 as well. For instance, the lowest points (T_N between 6.281 550 37 and 6.281 550 38) have $N = 6, 17, 22, 33, 44, 49, 60, 71, 82, 87, 98$; the distances between them are given by $\Delta N = 11, 5, 11, 11, 5, 11, 11, 11, 5, 11$ (note that $11 + 11 + 5 = 27$).

To explain regularities in figure 9 we compute $\nu_5 = 0.039$, $\nu_{22} = -0.029$, $\nu_{27} = 0.0093$, $\nu_{49} = -0.020$, $\nu_{76} = -0.011$, $\nu_{103} = -0.0015$, $\nu_{130} = 0.0078$ and also $\nu_{645} = 0.000\,10$. In this case the structure is also quite complicated because we have several candidates for periods. Some of them admit a clear interpretation. Joining every fifth point we get five sinusoidal curves with the period 130. Thus the distance between neighbouring 'sinusoids' is 26 which is very close to the period 27. The subsequent minima are at $N = 3, 25, 52, 79, 106, 128, 155, 182, 209$, therefore $\Delta N = 22, 27, 27, 27, 22, 27, 27, 27$ (note that $|\nu_{22}|$ is also relatively small). Looking at configurations of points near every minimum we can notice a distinct periodicity with the period 103.

Example 3 (Suris1 scheme, $\varepsilon = 0.1$, $p_0 = 0.05$, $T \approx 6.297\,237\,95$)**.** In this case the structure of figure 10 is extremaly simple (a single discrete curve). It can be explained by the non-existence of any 'small' periods. The smallest one, distinctly seen in figure 10, is 36. Namely, $\mu_{36} = 0.0057$, $\mu_{145} = 0.0050$, $\mu_{181} = 0.000\,69$. The period 181 is even more exact than the period 36 (μ_{181} is much smaller than μ_{36}). Therefore, after every five basic periods ($181 \approx 5 \times 36$) the periodicity improves.

Figure 11 consists of two intersecting discrete curves (periodic with the period 72), because $\nu_2 = -0.028$ is relatively small and $\nu_{72} = 0.0057$. Actually the important point is that $\nu_3 = 0.46$ is much greater than $|\nu_2|$. Note that $\mu_2 = -0.055$ is also not very large but $\mu_3 = -0.083$ is of the same order. The whole structure has the period 36 but (similarly as in example 1) the difference between A_{N+36} and A_N is quite large; A_N is close to A_{N+35} and A_{N+37} ($\nu_{35} = 0.017$, $\nu_{37} = -0.011$). Moreover, we have the period 181, quite accurate ($\nu_{181} = 0.000\,34$). This periodicity can be noted by looking at the minima or at points where the discrete curves 'intersect'.

Similar remarks concern the case presented in figures 1–3, where $T \approx 11.888\,840\,05$ and $\mu_9 = -0.0044$, $\mu_{448} = 0.0035$, $\mu_{457} = -0.000\,93$. The pattern on any of these figures consists of nine discrete curves and is periodic with the period close to 457.

The behaviour described on the above examples is typical, and similar periodic phenomena can be observed for other discretizations and for other choices of parameters except for very small values of ε (e.g., $\varepsilon \leqslant 0.01$) when periodic oscillations are comparable or smaller than the round-off error (then the oscillations become chaotic with a very small amplitude).

10. Numerical estimates of the amplitude and the period

All discretizations considered in this paper are characterized by very good stability of their trajectories. Therefore, such quantities as an average period and (in the case of oscillating motions) average amplitude are well defined for every discretization (provided that we consider trajectories sufficiently far from the separatrix and ε is not too large, it is sufficient to assume $\varepsilon \leqslant 0.5$).

10.1. Average amplitude

Relative errors of the average amplitude are presented in table 2 (for $\varepsilon = 0.02$ and $\varepsilon = 0.5$). They were computed as differences between the numerical results and exact amplitudes given in terms of elliptic functions. One can immediately see that in any case the best results are given by both gradient schemes (and the worst ones are given by the Suris1 and Suris2 schemes). The relative error of the leap-frog and Suris' methods practically does not depend on p_0. The accuracy of gradient methods increases for larger p_0, both for $\varepsilon = 0.02$ and $\varepsilon = 0.5$. For small ε (e.g., $\varepsilon = 0.02$) also projection schemes yield very small errors, like 10^{-8} or 10^{-9} (similar as gradient methods). However, for some p_0 their accuracy is very high (e.g., for $p_0 = 1.6$) while for some other p_0 is relatively worse (e.g., for $p_0 = 0.8$).

The implicit midpoint rule is comparable to gradient methods but only for small p_0 (e.g., $p_0 < 0.1$). The leap-frog method, both Suris' discretizations and (for $p_0 > 1.6$) the implicit midpoint rule yield much larger errors (by four orders of magnitude).

For greater ε (e.g., $\varepsilon = 0.5$) the differences between the studied methods are much smaller (they differ at most by two orders of magnitude). Gradient methods are most accurate. The implicit midpoint rule has similar accuracy for $p_0 < 1.2$ while projection methods are not much worse for $p_0 > 1.8$. The leap-frog method and both Suris' methods have larger relative errors for any p_0. We point out, however, that even those 'large' errors are not so bad (only several percent) with the exception of p_0 approaching 2 (when these discretizations fail to reproduce properly even the qualitative behaviour).

Figure 13 illustrates the dependence of the average amplitude on ε for $p_0 = 1.8$. Gradient methods and (especially for $\varepsilon < 0.3$) projection methods are most accurate.

10.2. Average period

Relative errors for the average period are presented in table 3 and also in table 4 (in both cases for $\varepsilon = 0.02$ and $\varepsilon = 0.5$). For $p_0 < 0.5$ all discretizations except the modified discrete gradient method have similar relative errors (the Suris1 scheme is the worst among them). The modified discrete gradient methods are much better (for $p_0 \approx 0$ its error is smaller by four orders of magnitude, at least), compare figure 12 ($p_0 = 0.1$) and figure 14 ($p_0 = 0.02$).

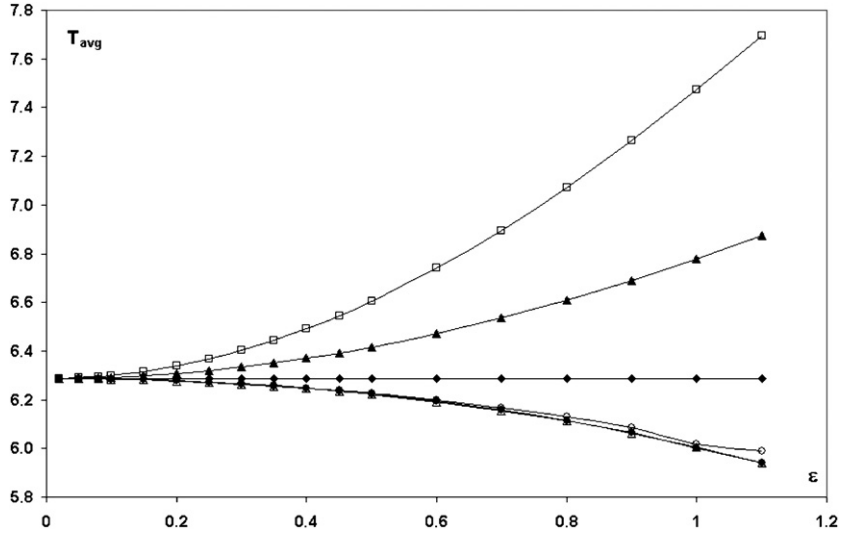

Figure 12. $T_{\mathrm{avg}} \equiv \bar{T}_{\mathrm{avg}}(0, 100, 200)$ as a function of ε for $p_0 = 0.1$ ($T_{\mathrm{th}} = 6.287\,117\,82$). White squares: Suris1, black triangles: midpoint (Suris2 and discrete gradient methods yield practically the same results), black diamonds: modified discrete gradient (very close to exact theoretical values), white triangles: leap-frog, black circles: symmetric projection, white circles: standard projection.

Table 2. Relative error of the averaged amplitude ($A = A_{\mathrm{avg}}(0, 50)$). The table contains $\log \frac{|A-A_{\mathrm{th}}|}{A_{\mathrm{th}}}$. We use traditional notation for common logarithms (e.g., $\bar{5}.70 \equiv -5 + 0.70$).

p_0	Leap-frog	Suris1	Suris2	Gradient	Modified gradient	Projection	Symmetric projection	Midpoint
				$\varepsilon = 0.02$				
0.05	$\bar{5}.70$	$\bar{4}.18$	$\bar{4}.00$	$\bar{8}.27$	$\bar{8}.27$	$\bar{8}.23$	$\bar{8}.23$	$\bar{8}.46$
0.1	$\bar{5}.70$	$\bar{4}.18$	$\bar{4}.00$	$\bar{8}.27$	$\bar{8}.26$	$\bar{8}.04$	$\bar{8}.08$	$\bar{8}.78$
0.3	$\bar{5}.70$	$\bar{4}.17$	$\bar{4}.00$	$\bar{8}.24$	$\bar{8}.23$	$\bar{8}.66$	$\bar{8}.71$	$\bar{7}.60$
0.5	$\bar{5}.70$	$\bar{4}.16$	$\bar{5}.99$	$\bar{8}.19$	$\bar{8}.20$	$\bar{8}.23$	$\bar{9}.93$	$\bar{6}.03$
0.8	$\bar{5}.70$	$\bar{4}.14$	$\bar{5}.98$	$\bar{9}.96$	$\bar{9}.92$	$\bar{7}.16$	$\bar{7}.31$	$\bar{6}.45$
1.2	$\bar{5}.71$	$\bar{4}.10$	$\bar{5}.95$	$\bar{9}.59$	$\bar{9}.59$	$\bar{9}.66$	$\bar{9}.34$	$\bar{6}.85$
1.6	$\bar{5}.75$	$\bar{4}.03$	$\bar{5}.92$	$\bar{9}.43$	$\bar{9}.43$	$\bar{1}0.73$	$\bar{8}.12$	$\bar{5}.18$
1.8	$\bar{5}.83$	$\bar{4}.01$	$\bar{5}.93$	$\bar{9}.61$	$\bar{9}.60$	$\bar{9}.66$	$\bar{9}.61$	$\bar{5}.40$
				$\varepsilon = 0.5$				
0.05	$\bar{2}.40$	$\bar{2}.93$	$\bar{2}.75$	$\bar{3}.80$	$\bar{3}.84$	$\bar{2}.50$	$\bar{2}.50$	$\bar{3}.80$
0.1	$\bar{2}.41$	$\bar{2}.93$	$\bar{2}.75$	$\bar{3}.80$	$\bar{3}.83$	$\bar{2}.48$	$\bar{2}.50$	$\bar{3}.80$
0.3	$\bar{2}.41$	$\bar{2}.93$	$\bar{2}.75$	$\bar{3}.78$	$\bar{3}.82$	$\bar{2}.41$	$\bar{2}.44$	$\bar{3}.80$
0.5	$\bar{2}.42$	$\bar{2}.92$	$\bar{2}.74$	$\bar{3}.76$	$\bar{3}.79$	$\bar{2}.16$	$\bar{2}.33$	$\bar{3}.80$
0.8	$\bar{2}.45$	$\bar{2}.91$	$\bar{2}.74$	$\bar{3}.66$	$\bar{3}.70$	$\bar{3}.95$	$\bar{3}.74$	$\bar{3}.79$
1.2	$\bar{2}.49$	$\bar{2}.87$	$\bar{2}.73$	$\bar{3}.39$	$\bar{3}.43$	$\bar{2}.53$	$\bar{2}.29$	$\bar{3}.82$
1.6	$\bar{2}.58$	$\bar{2}.81$	$\bar{2}.72$	$\bar{4}.26$	$\bar{4}.16$	$\bar{3}.97$	$\bar{2}.25$	$\bar{3}.95$
1.8	$\bar{2}.68$	$\bar{2}.79$	$\bar{2}.74$	$\bar{3}.09$	$\bar{3}.12$	$\bar{3}.75$	$\bar{3}.76$	$\bar{2}.13$

Then, with increasing p_0, all discretizations become to have similar accuracy with two very interesting exceptions: the leap-frog and implicit midpoint schemes have a kind of 'resonance

Table 3. Relative error of the averaged period ($T = \bar{T}_{\mathrm{avg}}(0, 100, 200)$). The table contains $\log \frac{|T-T_{\mathrm{th}}|}{T_{\mathrm{th}}}$. We use traditional notation for common logarithms (e.g., $\bar{5}.22 \equiv -5 + 0.22$).

p_0	Leap-frog	Suris1	Suris2	Gradient	Modified gradient	Projection	Symmetric projection	Midpoint
				$\varepsilon = 0.02$				
0.02	$\bar{5}.22$	$\bar{5}.92$	$\bar{5}.52$	$\bar{5}.52$	$\bar{9}.52$	$\bar{5}.22$	$\bar{5}.22$	$\bar{5}.52$
0.05	$\bar{5}.22$	$\bar{5}.92$	$\bar{5}.52$	$\bar{5}.52$	$\bar{8}.32$	$\bar{5}.21$	$\bar{5}.22$	$\bar{5}.52$
0.1	$\bar{5}.22$	$\bar{5}.92$	$\bar{5}.52$	$\bar{5}.52$	$\bar{8}.92$	$\bar{5}.19$	$\bar{5}.20$	$\bar{5}.52$
0.3	$\bar{5}.20$	$\bar{5}.91$	$\bar{5}.52$	$\bar{5}.51$	$\bar{7}.88$	$\bar{6}.83$	$\bar{5}.00$	$\bar{5}.51$
0.5	$\bar{5}.16$	$\bar{5}.90$	$\bar{5}.51$	$\bar{5}.49$	$\bar{6}.32$	$\bar{5}.05$	$\bar{6}.23$	$\bar{5}.49$
0.8	$\bar{5}.03$	$\bar{5}.86$	$\bar{5}.49$	$\bar{5}.45$	$\bar{6}.74$	$\bar{5}.75$	$\bar{5}.50$	$\bar{5}.42$
1.0	$\bar{6}.84$	$\bar{5}.83$	$\bar{5}.48$	$\bar{5}.39$	$\bar{6}.94$	$\bar{5}.99$	$\bar{5}.78$	$\bar{5}.34$
1.2	$\bar{6}.17$	$\bar{5}.78$	$\bar{5}.47$	$\bar{5}.32$	$\bar{5}.10$	$\bar{4}.18$	$\bar{5}.99$	$\bar{5}.21$
1.4	$\bar{6}.84$	$\bar{5}.73$	$\bar{5}.48$	$\bar{5}.19$	$\bar{5}.25$	$\bar{4}.34$	$\bar{4}.16$	$\bar{6}.92$
1.6	$\bar{5}.33$	$\bar{5}.69$	$\bar{5}.55$	$\bar{6}.97$	$\bar{5}.38$	$\bar{4}.48$	$\bar{4}.32$	$\bar{6}.56$
1.8	$\bar{5}.75$	$\bar{5}.77$	$\bar{5}.76$	$\bar{7}.96$	$\bar{5}.51$	$\bar{4}.61$	$\bar{4}.46$	$\bar{5}.44$
1.95	$\bar{4}.34$	$\bar{4}.28$	$\bar{4}.31$	$\bar{6}.96$	$\bar{5}.63$	$\bar{4}.70$	$\bar{4}.57$	$\bar{4}.06$
2.05	$\bar{4}.39$	$\bar{4}.44$	$\bar{4}.42$	$\bar{5}.06$	$\bar{5}.65$	$\bar{6}.54$	$\bar{4}.20$	$\bar{4}.06$
2.2	$\bar{5}.97$	$\bar{4}.05$	$\bar{4}.01$	$\bar{6}.85$	$\bar{5}.61$	$\bar{5}.86$	$\bar{4}.02$	$\bar{5}.61$
2.5	$\bar{5}.76$	$\bar{5}.84$	$\bar{5}.80$	$\bar{6}.62$	$\bar{5}.57$	$\bar{4}.03$	$\bar{5}.83$	$\bar{5}.40$
3	$\bar{5}.65$	$\bar{5}.71$	$\bar{5}.68$	$\bar{6}.39$	$\bar{5}.55$	$\bar{4}.11$	$\bar{5}.62$	$\bar{5}.31$
5	$\bar{5}.56$	$\bar{5}.58$	$\bar{5}.57$	$\bar{7}.86$	$\bar{5}.53$	$\bar{4}.16$	$\bar{5}.16$	$\bar{5}.24$
				$\varepsilon = 0.5$				
0.02	$\bar{2}.03$	$\bar{2}.71$	$\bar{2}.31$	$\bar{2}.31$	$\bar{6}.31$	$\bar{2}.03$	$\bar{2}.03$	$\bar{2}.31$
0.05	$\bar{2}.03$	$\bar{2}.71$	$\bar{2}.31$	$\bar{2}.31$	$\bar{5}.10$	$\bar{2}.02$	$\bar{2}.03$	$\bar{2}.31$
0.1	$\bar{2}.03$	$\bar{2}.70$	$\bar{2}.31$	$\bar{2}.31$	$\bar{5}.70$	$\bar{3}.99$	$\bar{2}.01$	$\bar{2}.31$
0.3	$\bar{2}.00$	$\bar{2}.70$	$\bar{2}.31$	$\bar{2}.30$	$\bar{4}.66$	$\bar{3}.52$	$\bar{3}.88$	$\bar{2}.30$
0.5	$\bar{3}.96$	$\bar{2}.68$	$\bar{2}.30$	$\bar{2}.29$	$\bar{3}.10$	$\bar{2}.00$	$\bar{3}.23$	$\bar{2}.28$
0.8	$\bar{3}.83$	$\bar{2}.64$	$\bar{2}.28$	$\bar{2}.24$	$\bar{3}.52$	$\bar{2}.65$	$\bar{2}.15$	$\bar{2}.21$
1	$\bar{3}.62$	$\bar{2}.60$	$\bar{2}.26$	$\bar{2}.18$	$\bar{3}.72$	$\bar{2}.89$	$\bar{2}.49$	$\bar{2}.14$
1.2	$\bar{4}.61$	$\bar{2}.55$	$\bar{2}.25$	$\bar{2}.11$	$\bar{3}.89$	$\bar{1}.09$	$\bar{2}.74$	$\bar{2}.01$
1.4	$\bar{3}.73$	$\bar{2}.49$	$\bar{2}.26$	$\bar{3}.99$	$\bar{2}.04$	$\bar{1}.26$	$\bar{2}.96$	$\bar{3}.75$
1.6	$\bar{2}.38$	$\bar{2}.57$	$\bar{2}.49$	$\bar{3}.93$	$\bar{2}.33$	$\bar{1}.61$	$\bar{1}.33$	$\bar{3}.28$
1.8	$\bar{2}.63$	$\bar{2}.51$	$\bar{2}.58$	$\bar{4}.81$	$\bar{2}.31$	$\bar{1}.50$	$\bar{1}.34$	$\bar{2}.19$
1.95	$\bar{1}.53$	$\bar{1}.27$	$\bar{1}.41$	$\bar{3}.76$	$\bar{2}.43$	$\bar{1}.46$	$\bar{1}.49$	$\bar{2}.77$
2.05	$\bar{1}.07$	$\bar{1}.08$	$\bar{1}.08$	$\bar{3}.86$	$\bar{2}.45$	$\bar{2}.60$	$\bar{1}.06$	$\bar{2}.96$
2.2	$\bar{2}.75$	$\bar{2}.77$	$\bar{2}.76$	$\bar{3}.65$	$\bar{2}.41$	$\bar{2}.65$	$\bar{2}.91$	$\bar{2}.43$
2.5	$\bar{2}.57$	$\bar{2}.59$	$\bar{2}.58$	$\bar{3}.43$	$\bar{2}.37$	$\bar{2}.70$	$\bar{2}.74$	$\bar{2}.21$
3	$\bar{2}.47$	$\bar{2}.47$	$\bar{2}.47$	$\bar{3}.20$	$\bar{2}.35$	$\bar{2}.74$	$\bar{2}.52$	$\bar{2}.13$
5	$\bar{2}.43$	$\bar{2}.36$	$\bar{2}.40$	$\bar{4}.70$	$\bar{2}.33$	$\bar{2}.74$	$\bar{3}.64$	$\bar{2}.11$

values' for which their accuracy is much better than the accuracy of all other method. Figure 15 shows how accurate is the leap-frog scheme for $p_0 = 1.21$ and for practically any ε. There are shown also next two discretizations: implicit midpoint and modified discrete gradient, much worse (for this value of p_0) than leap-frog (other discretizations are even less accurate). The implicit midpoint scheme has an analogical 'resonance value', namely $p_0 \approx 1.6$. It is worthwhile to point out that, surprisingly, projections applied to the leap-frog method have a strong negative effect on the accuracy of the average period for $0.8 < p_0 < 1.8$, especially for larger ε (e.g., $\varepsilon = 0.5$).

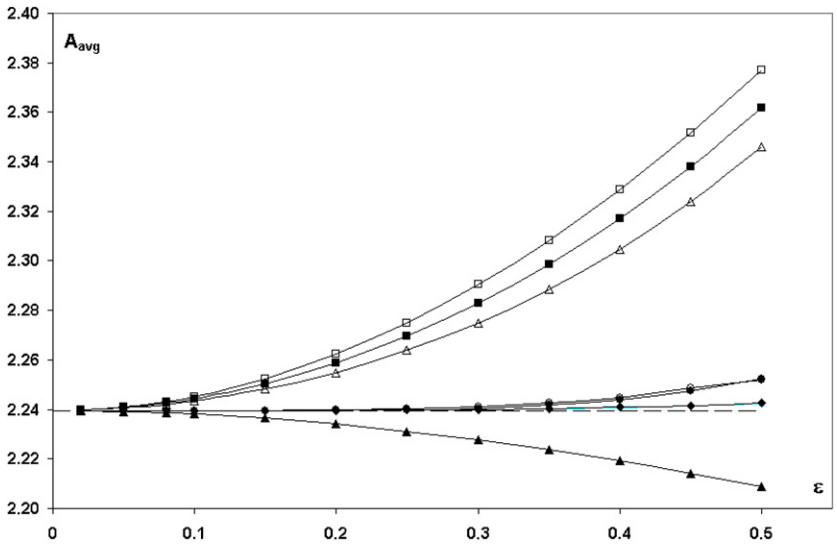

Figure 13. $A_{\mathrm{avg}} \equiv A_{\mathrm{avg}}(0, 50)$ as a function of ε for $p_0 = 1.8$ ($A_{\mathrm{th}} = 2.239\,539$). White triangles: leap-frog, black triangles: implicit midpoint, white squares: Suris1, black squares: Suris2, black diamonds: modified discrete gradient (discrete gradient method yields practically the same values), black circles: symmetric projection, white circles: standard projection (usually covered by black circles).

If p_0 approaches 2, then both gradient methods become more accurate than other methods (only for small ε, the projection methods are better). For p_0 very close to this limiting value the accuracy of all methods decreases rapidly, and the leap-frog method and both Suris' methods produce rotating motions instead of oscillations; see table 4. The closest neighbourhood of the separatrix ($p_0 = 2$) is discussed in more detail below. Here we remark only that, for p_0 slightly greater than 2, the implicit midpoint method fails to reproduce rotations and has wrong qualitative behaviour (i.e., oscillations).

In the case of rotating motions, the relative error of the average period is very similar for all considered methods except the discrete gradient scheme which is better by one or two orders of magnitude.

11. Interesting special cases

In this section, we briefly present several points which seem to be encouraging to further studies.

11.1. Extrapolation $\varepsilon \to 0$

For all studied discretizations we expect

$$\lim_{\varepsilon\to 0} T(\varepsilon, p_0) = T_{\mathrm{th}}(p_0), \qquad \lim_{\varepsilon\to 0} A(\varepsilon, p_0) = A_{\mathrm{th}}(p_0), \tag{66}$$

where $T_{\mathrm{th}}(p_0)$, $A_{\mathrm{th}}(p_0)$ do not depend on the discretization and are equal to theoretical values computed from the analytic formula (in terms of elliptic functions); compare figures 12 and 13.

Let us analyse quantitatively the case presented in figure 12 (the exact period is $T_{\mathrm{th}} \approx 6.287\,117\,83$). Fitting third-order polynomials (very close to parabolas, in fact) to

Table 4. Relative error of the averaged period in the neighbourhood of the separatrix ($T = \bar{T}_{\mathrm{avg}}(0, 100, 200)$). The table contains $\log \frac{|T-T_{\mathrm{th}}|}{T_{\mathrm{th}}}$. We use traditional notation for common logarithms (e.g., $\bar{4}.95 \equiv -4 + 0.95$). The blank space with a dot means that the qualitative behaviour of the discretization is wrong.

p_0	Leap-frog	Suris1	Suris2	Gradient	Modified gradient	Projection	Symmetric projection	Midpoint
				$\varepsilon = 0.02$				
$2 - 10^{-2}$	$\bar{4}.95$	$\bar{4}.93$	$\bar{4}.94$	$\bar{5}.18$	$\bar{5}.68$	$\bar{4}.72$	$\bar{4}.61$	$\bar{4}.66$
$2 - 10^{-3}$	$\bar{3}.85$	$\bar{3}.85$	$\bar{3}.85$	$\bar{5}.29$	$\bar{5}.72$	$\bar{4}.71$	$\bar{4}.63$	$\bar{3}.53$
$2 - 10^{-4}$	$\bar{2}.96$	$\bar{2}.96$	$\bar{2}.96$	$\bar{5}.35$	$\bar{5}.75$	$\bar{4}.70$	$\bar{4}.64$	$\bar{2}.38$
$2 - 10^{-5}$	–	–	–	$\bar{5}.39$	$\bar{5}.75$	$\bar{4}.70$	$\bar{4}.64$	$\bar{1}.01$
$2 - 10^{-6}$	–	–	–	$\bar{5}.45$	$\bar{5}.76$	$\bar{4}.69$	$\bar{4}.65$	$\bar{1}.33$
$2 - 10^{-7}$	–	–	–	$\bar{5}.87$	$\bar{5}.32$	$\bar{4}.69$	$\bar{4}.65$	$\bar{1}.49$
$2 - 10^{-8}$	–	–	–	$\bar{4}.14$	$\bar{4}.06$	$\bar{4}.69$	$\bar{4}.65$	$\bar{1}.58$
$2 - 10^{-9}$	–	–	–	$\bar{3}.21$	$\bar{3}.07$	$\bar{4}.69$	$\bar{4}.65$	$\bar{1}.65$
$2 + 10^{-8}$	$\bar{1}.62$	$\bar{1}.62$	$\bar{1}.62$	$\bar{5}.71$	$\bar{6}.63$	$\bar{4}.45$	$\bar{4}.52$	–
$2 + 10^{-7}$	$\bar{1}.54$	$\bar{1}.54$	$\bar{1}.54$	$\bar{5}.20$	$\bar{5}.80$	$\bar{4}.41$	$\bar{4}.50$	–
$2 + 10^{-6}$	$\bar{1}.40$	$\bar{1}.40$	$\bar{1}.40$	$\bar{5}.46$	$\bar{5}.81$	$\bar{4}.36$	$\bar{4}.47$	–
$2 + 10^{-4}$	$\bar{2}.63$	$\bar{2}.63$	$\bar{2}.63$	$\bar{5}.35$	$\bar{5}.74$	$\bar{5}.95$	$\bar{4}.25$	$\bar{2}.53$
$2 + 10^{-3}$	$\bar{3}.82$	$\bar{3}.83$	$\bar{3}.83$	$\bar{5}.29$	$\bar{5}.72$	$\bar{4}.21$	$\bar{4}.43$	$\bar{3}.54$
$2 + 10^{-1}$	$\bar{4}.16$	$\bar{4}.24$	$\bar{4}.20$	$\bar{6}.97$	$\bar{5}.63$	$\bar{5}.59$	$\bar{4}.12$	$\bar{5}.82$
				$\varepsilon = 0.5$				
$2 - 10^{-2}$	–	–	–	$\bar{3}.98$	$\bar{2}.49$	$\bar{1}.35$	$\bar{1}.52$	$\bar{1}.19$
$2 - 10^{-3}$	–	–	–	$\bar{2}.09$	$\bar{2}.53$	$\bar{1}.20$	$\bar{1}.52$	$\bar{1}.51$
$2 - 10^{-4}$	–	–	–	$\bar{2}.15$	$\bar{2}.55$	$\bar{1}.08$	$\bar{1}.51$	$\bar{1}.65$
$2 - 10^{-5}$	–	–	–	$\bar{2}.18$	$\bar{2}.56$	$\bar{2}.96$	$\bar{1}.51$	$\bar{1}.73$
$2 - 10^{-6}$	–	–	–	$\bar{2}.21$	$\bar{2}.57$	$\bar{2}.85$	$\bar{1}.50$	$\bar{1}.78$
$2 - 10^{-7}$	–	–	–	$\bar{2}.22$	$\bar{2}.58$	$\bar{2}.77$	$\bar{1}.50$	$\bar{1}.81$
$2 - 10^{-8}$	–	–	–	$\bar{2}.24$	$\bar{2}.59$	$\bar{2}.65$	$\bar{1}.50$	$\bar{1}.84$
$2 - 10^{-9}$	–	–	–	$\bar{2}.24$	$\bar{2}.59$	$\bar{2}.55$	$\bar{1}.50$	$\bar{1}.86$
$2 + 10^{-8}$	$\bar{1}.86$	$\bar{1}.86$	$\bar{1}.86$	$\bar{2}.24$	$\bar{2}.59$	$\bar{2}.75$	$\bar{1}.38$	–
$2 + 10^{-7}$	$\bar{1}.84$	$\bar{1}.84$	$\bar{1}.84$	$\bar{2}.22$	$\bar{2}.58$	$\bar{2}.75$	$\bar{1}.37$	–
$2 + 10^{-6}$	$\bar{1}.81$	$\bar{1}.81$	$\bar{1}.81$	$\bar{2}.21$	$\bar{2}.57$	$\bar{2}.74$	$\bar{1}.35$	–
$2 + 10^{-4}$	$\bar{1}.71$	$\bar{1}.71$	$\bar{1}.71$	$\bar{2}.15$	$\bar{2}.55$	$\bar{2}.76$	$\bar{1}.29$	–
$2 + 10^{-3}$	$\bar{1}.60$	$\bar{1}.59$	$\bar{1}.60$	$\bar{2}.09$	$\bar{2}.53$	$\bar{2}.64$	$\bar{1}.26$	–
$2 + 10^{-1}$	$\bar{2}.91$	$\bar{2}.93$	$\bar{2}.92$	$\bar{3}.77$	$\bar{2}.43$	$\bar{2}.62$	$\bar{2}.99$	$\bar{2}.66$

12 points ($\varepsilon = 0.01, 0.02, \ldots, 0.11, 0.12$) we get

$$
\begin{aligned}
T &= -0.038\,67\varepsilon^3 + 1.310\,512\varepsilon^2 - 0.000\,1050\varepsilon + 6.287\,118\,75 \quad \text{(Suris1)},\\
T &= -0.009\,09\varepsilon^3 + 0.524\,053\varepsilon^2 - 0.000\,0247\varepsilon + 6.287\,118\,05 \quad \text{(Suris2)},\\
T &= -0.004\,75\varepsilon^3 - 0.260\,242\varepsilon^2 - 0.000\,0130\varepsilon + 6.287\,117\,94 \quad \text{(leap}-\text{frog)}.
\end{aligned}
\tag{67}
$$

The last terms estimate the exact period quite well. Taking 10^{-7} as a unit we compute their absolute errors as 9.2, 2.2 and 0.9, respectively. They are comparable with the errors at $\varepsilon = 0.001$ (given by 13.1, 5.2 and -2.6, respectively). The errors at $\varepsilon = 0.01$ (namely, 1307.2, 523.3 and 260.6) are higher by two orders of magnitude. The modified discrete gradient scheme (with the δ-correction) beats all other discretizations: its error at $\varepsilon = 0.01$ is only 1.3 (in the same units).

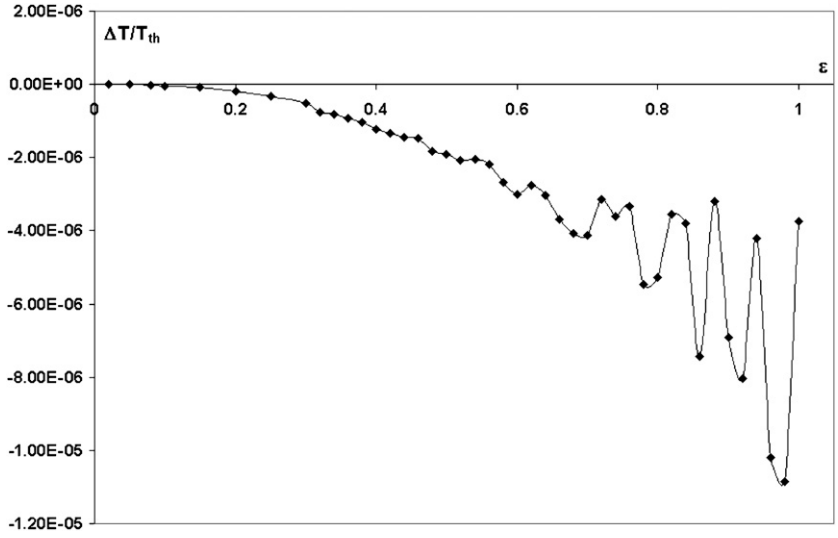

Figure 14. Modified discrete gradient method. Relative error of the period as a function of ε for $p_0 = 0.02$, $T_{\text{th}} = 6.283\,342\,395$, $T(\varepsilon) = T_{\text{avg}}(0, 30)$.

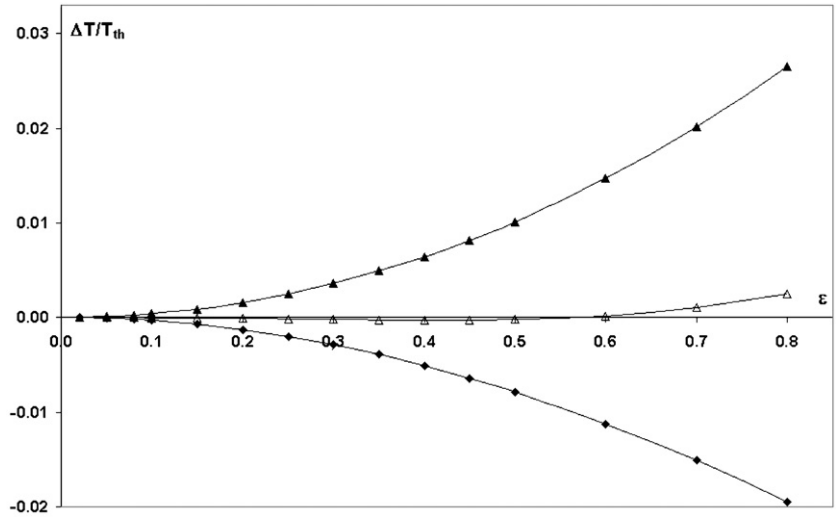

Figure 15. Relative error of the period as a function of ε for $p_0 = 1.21$ ('resonance value' for the leap-frog scheme), $T_{\text{th}} = 7.018\,661\,31087$, $T(\varepsilon) = \bar{T}_{\text{avg}}(0, 100, 200)$. Black triangles: implicit midpoint, white triangles; leap-frog, black diamonds: modified discrete gradient.

11.2. The neighbourhood of the separatrix

The separatrix is a border between oscillating and rotational motions. Table 4 presents the values of the period for motions near the separatrix, i.e., $p_0 \approx 2$. This is certainly the range of parameters, most difficult for accurate numerical simulations. The gradient schemes and projection methods yield satisfying results, especially for small ε, and are much better than all other methods. For rotating motions very close to the separatrix even projection methods

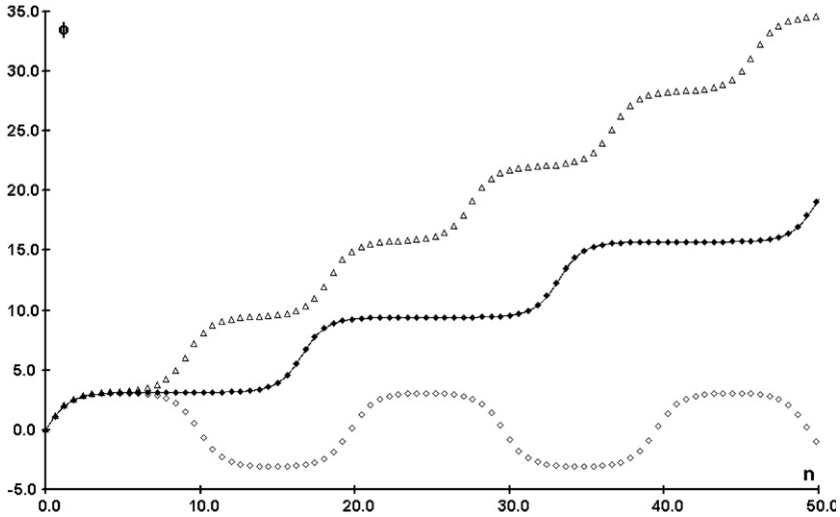

Figure 16. φ_n for $p_0 = 2.000\,001$, $\varepsilon = 0.1$. White triangles: leap-frog, black diamonds: modified discrete gradient, white diamonds: implicit midpoint. The period of the exact solution (continuous line): $T_{\text{th}} = 16.588\,095\,38$, the average period given by the modified discrete gradient scheme: $T = 16.563\,807\,22$.

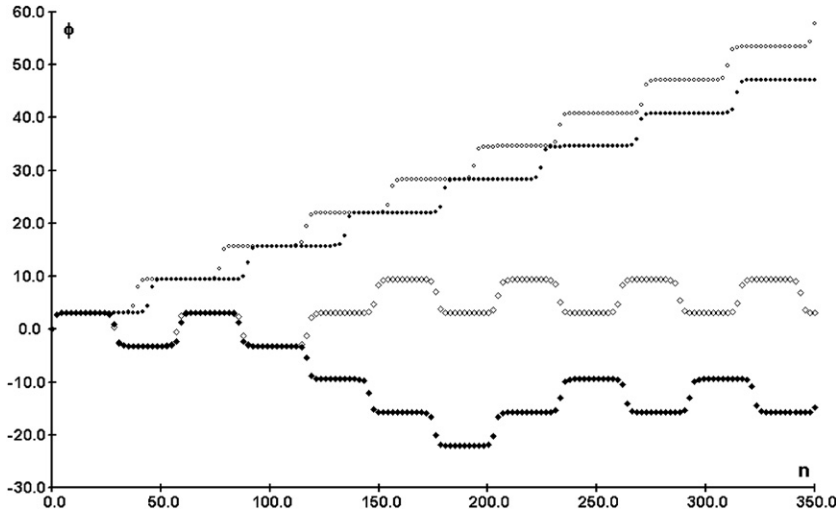

Figure 17. φ_n for $p_0 = 2, \varepsilon = 0.2$, the round-off error $\Delta = 10^{-16}$. White circles: standard projection, black circles: symmetric projection, white diamonds: discrete gradient, black diamonds: modified discrete gradient.

(especially the symmetric projection) become less accurate and only gradient methods yield relatively good quantitative results; see table 4.

The other discretizations can produce wrong results even qualitatively. Namely, the leap-frog and both Suris' schemes begin to simulate rotating motions for some $p_0 < 2$

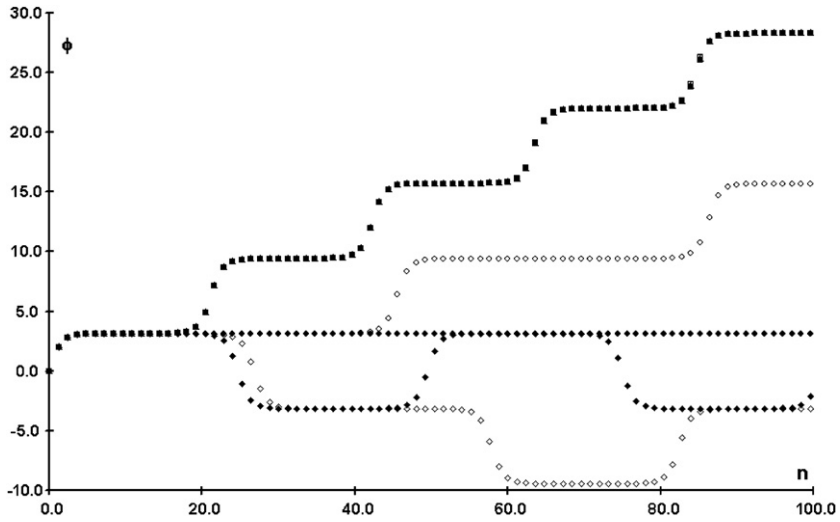

Figure 18. φ_n for $p_0 = 2$, $\varepsilon = 0.000\,25$, the round-off error $\Delta = 10^{-18}$. Black squares: Suris1, black circles: symmetric projection, white circles: standard projection, black diamonds: modified discrete gradient, white diamonds: discrete gradient. White squares (Suris2) and white triangles (leap-frog) are almost covered by black squares.

(e.g., for $p_0 = 1.99$ if $\varepsilon = 0.5$, and for $p_0 = 1.999\,99$ if $\varepsilon = 0.02$), while the implicit midpoint rule produces oscillating motions for some $p_0 > 2$ (e.g., for $p_0 = 2.000\,001$ if $\varepsilon = 0.02$, and for $p_0 = 2.001$ if $\varepsilon = 0.5$). For some initial data the leap-frog scheme produces chaotic trajectories. Even in the case of good qualitative behaviour these methods yield very large relative errors, especially for larger ε (for $\varepsilon = 0.5$ and $|p_0 - 2| \leqslant 0.001$ the leap-frog, implicit midpoint and both Suris' schemes yield relative errors like 30%–70% and more.

If $p_0 = 2$, then (in the continuous case) we have the motion along the separatrix, i.e., $\varphi \to \pi$ for $t \to \infty$. For larger ε (e.g., $\varepsilon = 0.2$) this behaviour is not reproduced by any discretization. Interesting results are given by both gradient schemes; see figure 17 ($\varepsilon = 0.2$). The standard gradient scheme produces oscillations, but after three periods one rotation is performed. The modified discrete gradient scheme gives a strange motion: first oscillations (two periods), then backward rotation (three periods), forward rotation and the return to oscillations. This picture depends on ε and the round-off error chosen. In any case, for both gradient schemes, we have a number of chaotic-looking switches between oscillations and rotations in both directions. Qualitatively this behaviour may be considered as satisfying. It reflects the fact that the equilibrium at $\varphi = \pi$ is unstable. In the same time, the projective discretizations (quite good at the qualitative description of motions near the separatrix) produce relatively slow rotational motion (similarly as the standard leap-frog method and both Suris schemes). However, for very small ε (e.g., $\varepsilon \leqslant 0.000\,25$) the symmetric projection method seems to have the proper qualitative behaviour and is much better than other considered numerical schemes; see figure 18.

11.3. Advantages of the new method

The discrete gradient method with δ-correction turned out to be very efficient as far as the numerical estimation of the period (for relatively small amplitudes) is concerned. The range

of these 'small' amplitudes is quite large, up to $\varphi \approx \pi/4$, which corresponds to $p_0 < 0.8$. Thus it contains also the cases which cannot be approximated by the linear oscillator. Even for $p_0 \approx 0.8$ the new method is several times better than the best of other considered schemes, and for smaller p_0 it becomes better even by four orders of magnitude (e.g., for $p_0 = 0.02$ the errors of other discretizations are greater by the factor at least 0.5×10^4; see table 3).

Figure 12 ($p_0 = 0.1$) shows how precise is the period given by our new method in comparison to the period given by other numerical schemes. Similarly, figure 14 presents the relative error for $p_0 = 0.02$ and a large range of ε. We see that even for $\varepsilon = 1$ the relative error is only 10^{-5}! For small ε the error is 10^{-9} and less.

Our method works very well also for larger amplitudes, but for p_0 larger than 1.4 the discrete gradient method is better, and the leap-frog scheme and implicit midpoint are unbeatable around their 'resonance' amplitudes ($p_0 \approx 1.2$ and $p_0 \approx 1.6$, respectively). In the case $p_0 > 2$ the δ-correction has negative influence on the accuracy of the gradient discretization (which is the best for rotating motions). However, the accuracy of the modified discrete gradient method is on the same level as the accuracy of all other considered methods.

In the close neighbourhood of the separatrix the modified discrete gradient scheme behaves similarly to the discrete gradient method and its qualitative behaviour is perfect. What is more, also the quantitative results are very good (compare table 4). Figure 16 compares the behaviour of our method with the leap-frog and implicit midpoint schemes for $p_0 = 2.000\,001$. The points generated by the modified discrete gradient method practically coincide with the exact solution (the relative error of the period is 0.59%), almost as good result as that given by the discrete gradient scheme (the error is 0.25%). The leap-frog scheme produces good qualitative behaviour but with the period two times smaller than the exact one. The implicit midpoint scheme gives wrong qualitative result: oscillations instead of rotation.

12. Summary

All methods considered in this paper are characterized by very high stability of generated periodic motions (provided that ε is not too large). They are much more stable than, for instance, non-symplectic Runge–Kutta methods, even of high order. The average period is practically constant for very long time, with the accuracy at least 10^{-7}, (we checked even several millions of periods). The period and the amplitude, as functions of time, perform regular small oscillations (relatively larger for projection methods). The periodic character of these oscillations turns out to be of a systematic origin, and we explained it considering rational approximations (with possibly small denominators) of the real numbers T/ε and $T/(2\varepsilon)$; see section 9.

The main aim of this paper was the comparison of several numerical schemes; the details are contained in sections 10 and 11. Here we point out some most typical features.

- **Stability**
  - All considered methods (except, to some extent, projection methods) yield very stable values of the period and the amplitude.
  - Projection methods give periods and amplitudes which are stable after averaging, but with large oscillations around the average (for small ε the oscillations decrease considerably), compare figure 5.
- **Accuracy of the period**
  Outside the separatrix neighbourhood (see table 3):
  - all methods (with small exceptions, see the following items) have relative errors of almost the same order (ε-dependent),

  - for small p_0 the modified discrete gradient scheme is better by four orders of magnitude than all other methods,
  - for rotational motions the discrete gradient method is usually the best (especially for large ε and p_0), better up to two orders of magnitude.

  In the neighbourhood of the separatrix (see table 4)

  - both gradient methods give very good results,
  - both projection methods give good results for $p_0 < 2$,
  - the best simulation of the motion along the separatrix is given by the symmetric projection method (for very small ε); see figure 18,
  - the leap-frog, implicit midpoint and both Suris' methods yield wrong results.

- **Accuracy of the amplitude**
  - For larger ε all methods have accuracy of the same order; see table 2. Gradient methods are slightly better, while the leap-frog and both Suris' schemes are worse than other methods.
  - For smaller ε we can divide the methods into two groups: less accurate (leap-frog and both Suris methods) and more accurate (gradient methods and projection methods), better by three orders of magnitude. The implicit midpoint rule belongs to the first group for larger p_0, and to the second group for small p_0.

The standard leap-frog method, although non-integrable, is quite good when compared with other, more sophisticated, discretizations. Its performance should be enhanced by the use of projection methods which impose the conservation of the energy integral. The projections work very well for small values of the time step, while for larger time steps they produce relatively large fluctuations of the period and the amplitude. In any case the projections produce much more accurate values of the average amplitude. The average period is similar to the period given by the standard leap-frog method: a little bit better in the case of oscillating motions, but slightly less accurate for rotating motions.

Surprising resonances occur for $p_0 \approx 1.21$ (for the leap-frog method) and $p_0 = 1.6$ (for the implicit midpoint rule). In the neighbourhood of these 'resonance' values these methods have exclusively high accuracy of the estimated period (practically for any ε), much better than all other methods. It would be interesting to explain this phenomenon.

Discretizations found by Suris [25] are very stable but produce relatively large errors as compared to other numerical schemes. This is surprising because these methods are both integrable and symplectic. Probably the large error (large deviation from the exact solution) seems to be of a systematic origin. We plan to construct appropriate modifications of Suris' discretizations in order to enhance their precision without destroying their stability.

The discrete gradient method is (for any ε and any p_0) among the most accurate methods. We proposed a modification of the discrete gradient method which proved to be quite successful, especially when applied to oscillating motions. Our new method is extremely efficient for small oscillations. The relative error of the period computed by this method is less at least by four orders of magnitude in comparison with other considered numerical schemes.

Acknowledgments

The authors are grateful to Professor Grzegorz Sitarski for useful comments and turning our attention on [4, 9]. The first author was partially supported by the Polish Ministry of Science and Higher Education (grant no 1 P03B 017 28).

References

[1] Agarwal R P 2000 *Difference Equations and Inequalities* (New York: Dekker) chapter 3

[2] Ascher U and Reich S 1999 On some difficulties in integrating highly oscillatory Hamiltonian systems *Computational Molecular Dynamics* (*Lect. Notes Comput. Sci. Eng.*) (Berlin: Springer) pp 281–96

[3] Benettin G and Giorgilli A 1994 On the Hamiltonian interpolation of near to the identity symplectic mappings with application to symplectic integration algorithms *J. Stat. Phys.* **74** 1117–43

[4] Breiter S, Fouchard M, Ratajczak R and Borczyk W 2007 Two fast integrators for the galactic tide effects in the Oort cloud *Mon. Not. R. Astron. Soc.* **377** 1151–62

[5] Cieśliński J L 2007 An orbit-preserving discretization of the classical Kepler problem *Phys. Lett.* A **370** 8–12

[6] Cieśliński J L and Ratkiewicz B 2005 On simulations of the classical harmonic oscillator equation by difference equations arXiv:phy/0507182
Cieśliński J L and Ratkiewicz B 2006 *Adv. Difference Equ.* **2006** 40171

[7] Friedman A and Auerbach S P 1991 Numerically induced stochasticity *J. Comput. Phys.* **93** 171–88

[8] Gonzales O 1996 Time integration and discrete Hamiltonian systems *J. Nonlinear Sci.* **6** 449–67

[9] Goździewski K, Breiter S and Borczyk W 2008 The long-term stability of extrasolar system HD 37124. Numerical study of resonance effects *Mon. Not. R. Astron. Soc.* **383** 989–99

[10] Hairer E 2000 Symmetric projection methods for differential equations on manifolds *BIT* **40** 726–34

[11] Hairer E, Lubich C and Wanner G 2006 *Geometric Numerical Integration: Structure-preserving Algorithms for Ordinary Differential Equations* 2nd edn (Berlin: Springer)

[12] Iserles A 1997 Insight, not just numbers *Proc. 15th IMACS World Congress* vol 2 ed A Sydow (Berlin: Wissenschaft & Technik Verlag) pp 589–94

[13] Iserles A 2001 Multistep methods on manifolds *IMA J. Numer. Anal.* **21** 407–19

[14] Iserles A and Zanna A Qualitative numerical analysis of ordinary differential equations *The Mathematics of Numerical Analysis* (*Lect. Appl. Math.*) ed J Renegar (Providence RI: American Mathematical Society)

[15] Itoh T and Abe K *et al* 1988 Hamiltonian conserving discrete ca–ical equations based on variational difference quotients *J. Comput. Phys.* **77** 85–102

[16] LaBudde R A and Greenspan D 1974 Discrete mechanics—a general treatment *J. Comput. Phys.* **15** 134–67

[17] Leimkuhler B and Reich S 2004 *Simulating Hamiltonian Dynamics* (Cambridge: Cambridge University Press)

[18] McLachlan R I, Perlmutter M and Quispel G R W 2004 On the nonlinear stability of symplectic integrators *BIT* **44** 99–117

[19] McLachlan R I and Quispel G R W 2006 Geometric integrators for ODEs *J. Phys. A: Math. Gen.* **39** 5251–85

[20] McLachlan R I, Quispel G R W and Robidoux N 1998 A unified approach to Hamiltonian systems, Poisson systems, gradient systems and systems with Lyapunov functions and or first integrals *Phys. Rev. Lett.* **81** 2399–403

[21] McLachlan R I, Quispel G R W and Robidoux N 1999 Geometric integration using discrete gradients *Phil. Trans. R. Soc.* A **357** 1021–45

[22] Quispel G R W and Capel H W 1996 Solving ODE's numerically while preserving a first integral *Phys. Lett.* A **218** 223–8

[23] Quispel G R W and Turner G S 1996 Discrete gradient methods for solving ODE's numerically while preserving a first integral *J. Phys. A: Math. Gen.* **29** L341–9

[24] Reid J G 1983 *Linear System Fundamentals, Continuous and Discrete, Classic amd Modern* (New York: McGraw-Hill)

[25] Suris Yu B 1989 On integrable standard-like mappings *Funct. Anal. Appl.* **23** 74–6

[26] Suris Yu B 2003 *The Problem of Integrable Discretization: Hamiltonian Approach* (Basel: Birkhäuser) chapter 20

[27] Sussman G J and Wisdom J 1992 Chaotic evolution of the solar system *Science* **257** 56–62

[28] Wisdom J and Holman M 1991 Symplectic maps for the *N*-body problem *Astron. J.* **102** 1528–38

[29] Yoshida H 1993 Recent progress in the theory and application of symplectic integrators *Celest. Mech. Dynam. Astron.* **56** 27–43